BSC

Engineering Change Notice

Complete only applicable items.

3. Document Identifier:	4. Rev.:	5. Title:	6. ECN:
CAL-WIS-AC-000001	0B	Mechanical Assessment of the Waste Package Subject to Vibratory Ground Motion	1

7. Reason for Change:
Changes are being made to resolve editorial comments resulting from an AP-7.5Q deliverable review.

8. Supersedes Change Document: ☐ Yes If, Yes, Change Doc.: _____ ☒ No

9. Change Impact:

Inputs Changed:	☐ Yes	☒ No	Results Impacted:	☐ Yes	☒ No
Assumptions Changed:	☐ Yes	☒ No	Design Impacted:	☐ Yes	☒ No

10. Description of Change: (Address any "Yes" answers)

Page 5-28: In the first sentence of Section 5.4.3.1 delete the "a" before "standard engineering practice."

"Following a standard engineering practice, the mesh of the OCB in the FE mesh is refined in the region where significant deformations and residual stresses are expected (i.e., region of interest)."

is replaced by:

"Following standard engineering practice, the mesh of the OCB in the FE mesh is refined in the region where significant deformations and residual stresses are expected (i.e., region of interest)."

Page 5-46: Add a period to the sentence at the end of the page.

"The largest impact velocity of 13.4 m/s is recorded for realization 10"

is replaced by:

"The largest impact velocity of 13.4 m/s is recorded for realization 10."

Page 5-50: Table 5-8.

In the row with the Name "Glancing", in the cell under the column "Vz" precede the value of "5.720" by a minus sign "(–)".

is replaced by:

"Glancing" row, Column Vz, value should read –5.720.

Page 5-62: In the first sentence of the second paragraph, change "approximation" to "approximations."

"To investigate the effects of these approximation, additional discontinuum analyses using the software UDEC version 3.1 (BSC 2002 [DIRS 161949], STN: 10173-3.1-00) were carried out."

is replaced by:

"To investigate the effects of these approximations, additional discontinuum analyses using the software UDEC version 3.1 (BSC 2002 [DIRS 161949], STN: 10173-3.1-00) were carried out."

Page VI-3: Figure VI-2: Add note to clarify the view and add unit vector to figure with X and Z directions noted.

addition should read:

"NOTE: This is a plan view looking down on a waste package underneath a drip shield."

Page VI-5: Table VI-1.

In the row with the Name "Glancing", in the cell under the column "Vz" precede the value "5.720" by a minus sign "(–)".

is replaced by:

"Glancing" row, Column Vz, value should read –5.720.

3. Document Identifier:	4. Rev.:	5. Title:	6. ECN:
CAL-WIS-AC-000001	0B	Mechanical Assessment of the Waste Package Subject to Vibratory Ground Motion	1

10. Description of Change: (Address any "Yes" answers) (CONTINUED)

Page VI-23: Add missing space between "plate" and "2" in first paragraph of Section VI-3.2, and delete space between Figures VI-18 (a).

"The maximum Von-Mises stress plots presented in Figures VI-18 (a) to VI-32(a) demonstrate that the stress values in bulkhead, large support beam, plate 1, and plate2) remain within their respective material's true ultimate strength (Table 5-1)."

is replaced by:

"The maximum Von-Mises stress plots presented in Figures VI-18(a) to VI-32(a) demonstrate that the stress values in bulkhead, large support beam, plate 1, and plate 2) remain within their respective material's true ultimate strength (Table 5-1)."

Page IX-4: Add missing words.

"An unexpected result is that sample taken from extraction window 3, with smallest porosity of 6.9 percent, exhibits the softest response."

is replaced by:

"An unexpected result is that the sample taken from extraction window 3, with the smallest porosity of 6.9 percent, exhibits the softest response."

Pages V-21, VI-26 through VI-41, VI-43 through VI-45, and VI-52: Figures VI-15, VI-18 through VI-33, VI-35 through VI-37, and VI-44: Add note to clarify drip shield elements corresponding to Curves A, B, C, and D.

"NOTE: Curve A is Plate 1, Curve B is Plate 2, Curve C is the large support beam, and Curve D is the bulkhead. See Figure VI-7."

Pages VI-46, VI-47 and VI-49: Figures VI-38, VI-39, and VI-42: Add note to clarify drip shield elements corresponding to Curves A, B, C, D, and E.

"NOTE: Curve A is Plate 1, Curve B is Plate 2, Curve C is the large support beam, Curve D is the bulkhead, and Curve E is the bulkhead flange. See Figures VI-6 and VI-7."

11. Originator: (Print/Sign/Date) Richard Quittmeyer	R.C. Quittmeyer	08/30/2005
Checker: (Print/Sign/Date) Ming Lin		08/30/2005
Approved: (Print/Sign/Date) Paul Dixon		8-30-05

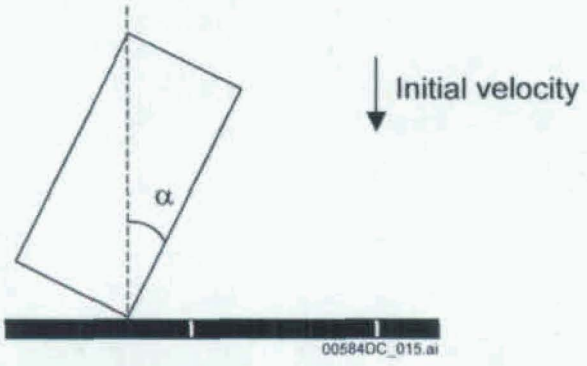

Source: BSC 2003 [DIRS 162293], Figure 2.

Figure 5-11. Initial Position of the Waste Package for the End Impacts

The selected impact velocities range from 1 m/s to 10 m/s and impact angles ranging from 0 to 8 degrees were anticipated to be sufficiently wide to encompass all velocities and angles encountered during simulations of waste package response to vibratory ground motion.

5.4.3.1 Numerical Representation

Following standard engineering practice, the mesh of the OCB in the FE mesh is refined in the region where significant deformations and residual stresses are expected (i.e., region of interest). The remaining part of the mesh is coarser to reduce the simulation running time. The extent of the region of interest depends on the input parameters (the velocity and angle of impact). The configuration for 5-degree end impact of the 21-PWR waste package is illustrated in Figure 5-12. A three-dimensional FE representation of the waste package was developed using the dimensions provided in *21-PWR Waste Package Side and End Impacts* (BSC 2003 [DIRS 162293], Attachment I). Detail of the FE representation of 21-PWR waste package for ideal (0 degree) end impact is illustrated in Figure 5-13.

The thickness of the OCB was reduced by 2 mm on its outer side (BSC 2003 [DIRS 162293], Assumption 3.14). The target surface was conservatively assumed to be elastic and unyielding, and its density was rounded up to 8,000 kg/m^3. A static and dynamic friction coefficient of 0.5 was taken into account between all parts. The value of 0.5 is an average value for the range of friction coefficient, 0.2 to 0.8, defined in Assumption 3.2.4 and used for the structural response calculations described in Section 5.2.1. The use of an average friction coefficient of 0.5 is reasonable here because this is a single, discrete impact on an unyielding surface, so frictional forces should have a very minor effect in determining damaged area on the waste package. Other simplifications of the internal structure of the waste package are described in Attachment III.

Two sets of 17 ground motions, at 2.44-m/s and 5.35-m/s PGV levels, were analyzed. Ground motions at the 1.05-m/s PGV level do not result in impacts above the 0.85 m/s damage threshold (Assumption 3.2.29) between the waste package and drip shield. The full duration of the ground motions was not simulated. Instead, the portion of the records of the ground motions between the points corresponding to 5 and 95 percent in the energy build-up, as measured by the Arias intensity (Kramer 1996 [DIRS 103337], Section 3.3.4), was simulated. For each three-component set of ground motions (i.e., two horizontal and one vertical), these points were determined for each component; then, the earliest 5 percent point and the latest 95 percent point were used to define the duration of strong ground motion for that set of ground motions.

Geometry of the objects within the drift was simplified in the analyses to account for the important features related to the waste package-drip shield impact study (Assumption 3.2.3). The rationale of using the simplified geometry is provided in Attachment V, Section V-3.3. The mechanical properties used in the analyses are listed in Attachment V, Section V-3.4.

5.6.1.2 Results

Waste package-drip shield and waste package-emplacement pallet impacts were monitored during the dynamic simulations. Time of impact, location of impact (in the global coordinate system) and relative impact velocity were recorded for each impact. Snap-shots of the simulated geometry taken every 0.05 s during the simulation were used to generate animations showing evolution of the drift geometry (collapse) and interaction between the objects inside the drift. The relative impact velocities reported in the global coordinate system are calculated as the difference between the average velocities of the waste package and the drip shield.

The summary of the waste package-drip shield impact results is listed in Table 5-7. The table contains the number of impacts with impact velocity greater than 0.85 m/s (Assumption 3.2.29) and the magnitude of maximum impact velocities (if greater than 0.85 m/s). Snap-shots of the geometry of the simulated problem at 1-s time intervals for realization 10 at the 2.44-m/s and 5.35-m/s PGV levels are shown in Attachment V, Figures V-9 and V-10. As illustrated in Figure V-10 in the frame at 5 s, the waste package impacts the plates attached to the drip shield legs, but also, for ground motions with large vertical acceleration, impacts the waste package into the bulkhead region in the crown (from below) of the drip shield structure. At the 2.44-m/s PGV level, the waste package impacts (with impact velocity greater than 0.85 m/s) the drip shield in 4 of 17 realizations. In two cases, the maximum impact velocities are greater than 5 m/s; in the other two cases, the maximum impact velocities are less than 2 m/s. In only two realizations at the 5.35 PGV level does the waste package not impact the drip shield with impact velocity greater than 0.85 m/s. The maximum impact velocities at the 5.35-m/s PGV level vary significantly from one realization to another. The largest impact velocity of 13.4 m/s is recorded for realization 10.

The direction of impact—the motion of the waste package relative to the drip shield was examined. Table 5-8 summarizes the impact velocity direction parameters chosen for each of the contact locations. The impacts are classified as direct, glancing (impact to wall plates with large longitudinal velocity component), oblique (horizontal impact to walls with equal horizontal velocity components), falling and rising oblique (oblique, with upward or downward velocity component), vertical and vertical oblique directions.

Table 5-8. Impact Direction and Corresponding Velocity Values

Name	Directional Vector	Magnitude (m/s)	Vx	Vy	Vz
Direct	(1, 0, 0)	6.000	6.000	0	0
Glancing	(0.1, 0,–1)	6.000	0.572	0	–5.720
Oblique	(1, 0, –1)	6.000	4.243	0	–4.243
Falling Oblique	(1, –1, –1)	6.000	3.464	–3.464	–3.464
Rising Oblique	(1, 1, –1)	6.000	3.464	3.464	–3.464
Vertical	(0, 1,0)	6.000	0	6.000	0
Vertical Oblique	(1, 1,0)	6.000	4.243	4.243	0

The above velocity component directions were combined with both the 0° and 4° angular orientations of the waste package. Thus, a 4° orientation combined with a glancing velocity can result in a potential tearing or gouging mode of deformation along the sidewall plates. Additionally calculations in which the waste package "clips" a bulkhead beam at velocities of 1.00 m/s and 2.25 m/s were analyzed (Figure 5-21). This highly unlikely case (see Attachment VI for explanation) is viewed as an extreme test of drip shield stability as a waste package can severely bend and potentially destroy the support function of a bulkhead beam in this manner.

representing the average weight of the objects resting on the invert and the pressure due to the caved rock mass, was used in the calculations (Assumption 3.2.24). The numerical simulations indicate that in most cases the strong ground motions will induce PGV on top of the crushed tuff practically the same or insignificantly larger (within 5 percent) than the PGV of the free field (Tables VIII-4 to VIII-7). The increase in PGV and the number of cases with increased PGV is smaller for larger confinement and for less intense ground motions (i.e., the 2.44-m/s PGV level). The amplification, when it occurs, is associated with the high frequency portion of a motion and occurs over a relatively short duration of time.

The continuum analyses use two approximations that can potentially affect the analysis results:

- The crushed tuff in the invert of the emplacement drift is represented as a continuum material.

- The effect of the engineered systems inside the emplacement drift was taken into account by applying the vertical confining pressure on the crushed tuff.

To investigate the effects of these approximations, additional discontinuum analyses using the software UDEC version 3.1 (BSC 2002 [DIRS 161949], STN: 10173-3.1-00) were carried out. The discontinuum analyses, which represent the invert as a granular material, include explicit representation of the waste package, the emplacement pallet and the drip shield, and simulate collapse of the drift, show that the invert: a) deforms practically as a rigid body during ground motions from the 2.44-m/s PGV level, and b) undergoes irreversible deformation during ground motions from the 5.35-m/s PGV level. The irreversible deformation of the invert is probably overestimated in the numerical analysis, which represents the crushed tuff in the invert as a material with no porosity in the initial configuration (porosity for the crushed tuff was estimated to be around 31 percent). For the cases analyzed (both PGV levels) the maximum impact velocity (between the waste package and the emplacement pallet and the invert) and number of impacts decrease or remain the same if a deformable invert is assumed in the calculations, compared to the cases when the invert is represented as a rigid body.

The approach of representing the invert as a rigid body has relatively small effect on the ground motions to which the objects inside the emplacement drift are subjected. With relatively small effect, the representation of the invert as a rigid body is considered as justified and reasonable.

5.9 CONCLUSIONS

This calculation presents the results of analyses of the mechanical effects of postclosure vibratory ground motions on waste packages within the emplacement drift, and the additional effects that waste package movement may have on other engineered barrier components. The analyses included examination of the following effects:

- Waste package-to-waste package interactions and resulting damage to the lid area of the waste package

- Waste package-to-emplacement pallet interactions and resulting damage to the sides of the waste package

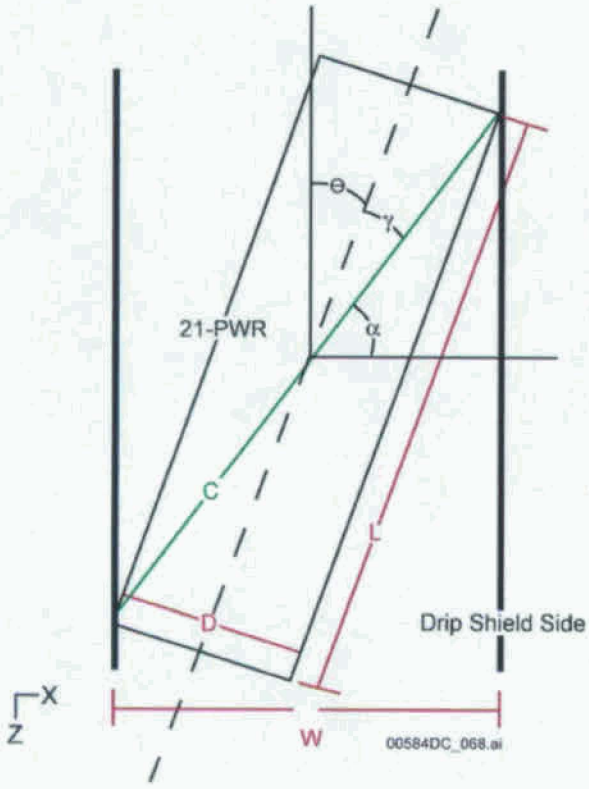

$D := 1.72 \cdot m \quad L := 4.99 \cdot m \quad W := 2.3 \cdot m$

$C := \sqrt{D^2 + L^2} \qquad C := 5.278 \cdot m$

$\cos(\alpha) = \frac{W}{C} \qquad \sin(\gamma) = \frac{D}{C}$

$\Theta := 90 \cdot deg - acos\left(\frac{W}{C}\right) - asin\left(\frac{D}{C}\right)$

$\Theta := 6.815\ deg$

Source: (Dimensions are from BSC 2005 [DIRS 173303] and BSC 2005 [DIRS 173501]).

NOTE: This is a plan view looking down on a waste package underneath a drip shield.

Figure VI-2. Maximum Articulation of the 21-PWR Waste Package

VI-2.1.2 Impact Location

While examining the kinematic analyses of multiple waste packages subjected to vibratory ground motion, it becomes obvious that just about any location inside the drip shield may be subjected to a waste package impact. From side (cross-drift) impacts to vertical impacts, the waste package is free to move around. Therefore, it is important to consider the most vulnerable locations where the waste package may hit. Locations of impacts considered (referring to Figures VI-3 and VI-7) are at Plate 2 directly supported by the large support beam (Segment 1, Direct impact location), Plate 2 centered between two large support beams (Segment 2 impact location), the bulkhead from underneath (Segment 1, vertical and vertical oblique), the bulkhead from the side (longitudinally; Bulkhead impact location), and a combination of those impacts. Due to the need for computational efficiency, different segments of the drip shield are modeled depending on the impact location. Segment 1 (between lines A and B in Figure VI-3) was used for impacts centered on the large support beam, vertical impacts to the bulkhead, and multiple impacts. Segment 2 (between lines C and D in Figure VI-3) was used for impacts centered between two large support beams. A triple segment FE representation (from end to end in Figure VI-3) was created for the simulation of longitudinal impacts to the bulkhead. The numerical representations of these segments are discussed at length in Section VI-2.2.

Therefore, impacts with resultant velocity greater than 6 m/s is considered unlikely, making it an appropriate upper bound. As the direction of the velocity vector changes (as explained in the next section), the velocity in a given direction changes, but the resultant magnitude remains constant.

VI-2.1.4 Direction of Impact

The final parameter considered was the direction the waste package is moving prior to impact. Seven directions are considered as listed in Table V1-1. The listed directions were chosen because of the potential they may have in causing unique stress loads causing collapse of the drip shield. The unit vector column, which corresponds to the model orientation in Figure VI-3, indicates which way the waste package is headed. The Vx, Vy, and Vz columns indicate the velocity in a given direction for the corresponding unit vector. As stated before, the resultant magnitude is held constant while the velocity in a given direction changes with the direction of the vector.

Table VI-1. Impact Direction and Corresponding Velocity Values

Name	(Directional Vector)	Magnitude (m/s)	Vx	Vy	Vz
Direct	(1,0,0)	6.000	6.000	0	0
Glancing	(0.1,0,-1)	6.000	0.572	0	-5.720
Oblique	(1,0,-1)	6.000	4.243	0	-4.243
Falling Oblique	(1,-1,-1)	6.000	3.464	-3.464	-3.464
Rising Oblique	(1,1,-1)	6.000	3.464	3.464	-3.464
Vertical	(0,1,0)	6.000	0	6.000	0
Vertical Oblique	(1,1,0)	6.000	4.243	4.243	0

NOTE: Because of segment symmetry conditions, the 0° waste package orientation for Segment 1 and 2 provides the same loading conditions (repeated the length of the drift). Therefore, analysis for 0° orientation is not necessary for Segment 2. The corner of the waste package (i.e. 4° orientation) impacting the underside of drip shield is considered an extraneous possibility therefore not considered in the parametric analyses.

VI-2.1.5 Parametric Analysis Summary

Table VI-2 couples the waste package orientation, impact location, and velocity direction in one matrix. In total there are 16 scenarios analyzed for the parametric study. It should be noted that the stress and displacement results for the glancing cases of Segment 1 were small enough not to need consideration for Segment 2.

Table VI-5. Maximum Von-Mises Stress (MPa) for Direct 4° Impacts

	Plate 1	Plate 2	Large Support Beam	Bulkhead
One Segment	212	270	825	742
Triple Segments	215	310	822	759
% Difference	1.40	12.9	0.49	2.24

Table VI-6. Final Displacement (m) for Direct 4° Impacts

	Absolute		Relative to Rubble	
	Left	Right	Left	Right
One Segment	0.000	0.081	0.000	0.055
Triple Segments	0.000	0.014	0.000	0.007
% Difference	0.0	479	0.0	686

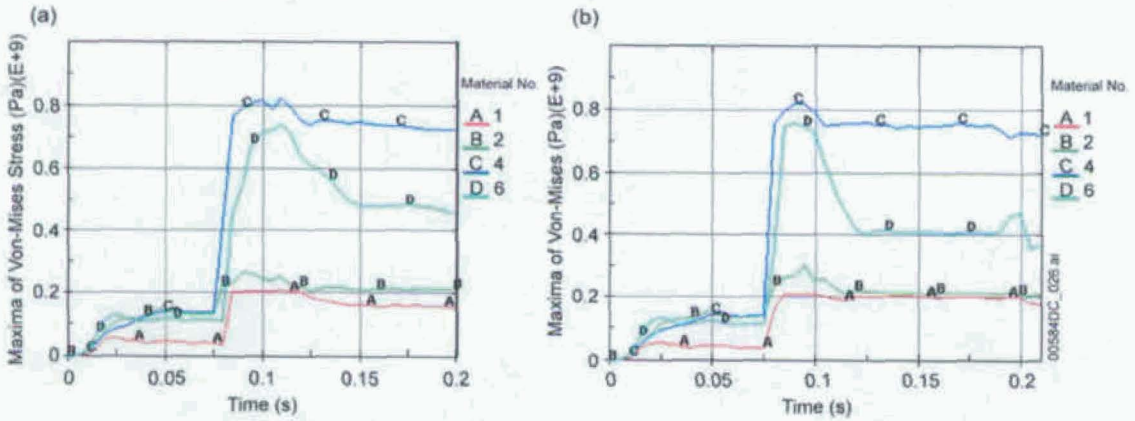

NOTE: Curve A is Plate 1, Curve B is Plate 2, Curve C is the large support beam, and Curve D is the bulkhead. See Figure VI-7.

Figure VI-15. X-Direct Impact: Maximum Von-Mises Stress (Pa) in the Drip Shield Plates, Bulkhead and Large Support Beams Drip Shield Structural Members (a) Segment 1 (b) Triple Segment

Most of the values in Tables VI-4 and VI-5 have small percent differences between the two segments; the values that deviate are the maximum stress for plate 2 and the final displacement for the right side of the drip shield. Examining the displacement contours of the drip shield (Figures VI-16 and VI-17) gives insight to the phenomena causing these differences. These figures show the drip shields segments at their maximum displacements. Notice the displacement contours span the entire length for Segment 1, and remain localized for the Triple Segment. The line-loading conditions in Segment 1 cause displacement across the entire segment, which causes the bottom of plate 2 to lift off of the invert. When the bottom of plate 2 lifts off the invert, higher displacements occur because the plate no longer has to overcome frictional forces with the invert to move. This phenomenon explains the two orders of magnitude difference between the displacement of Segment 1 and the Triple Segment. Also, with the entire segment displacing, the stresses in Segment 1 are distributed across plate 2, where the triple segment experiences more localized stresses (which explains the higher maximum stress in the Triple Segment).

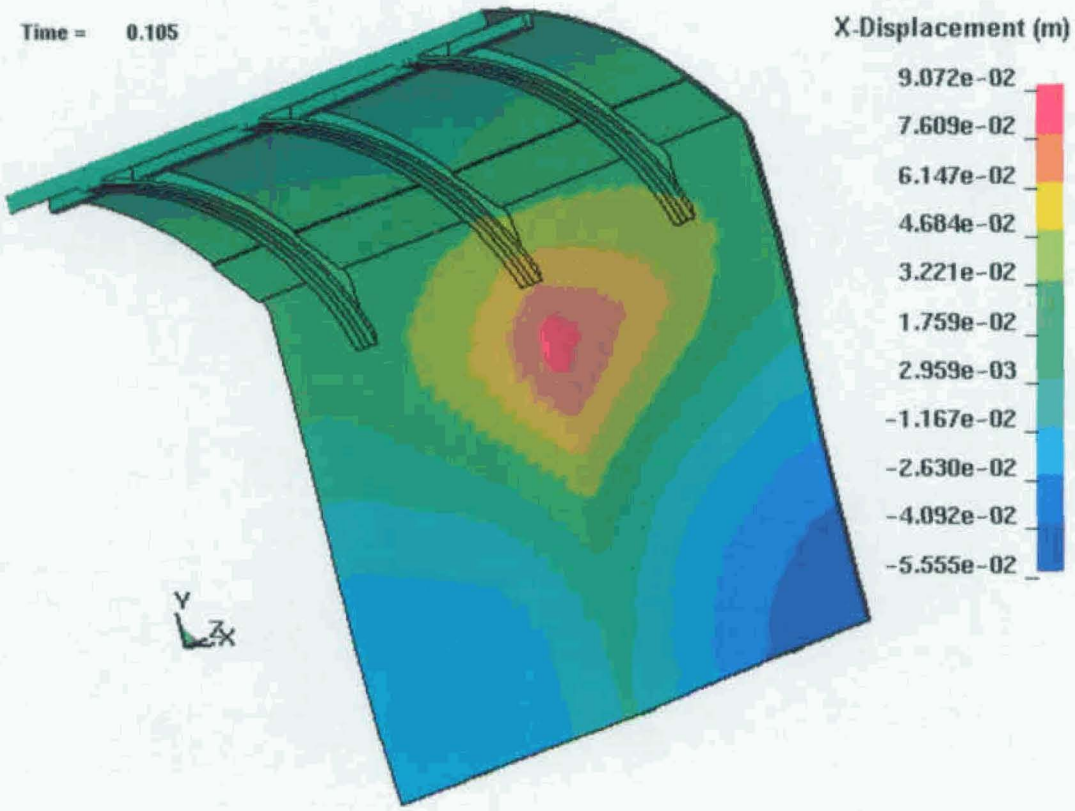

Figure VI-17. X-Displacement Contours for the Triple Segment During a 6 m/s Direct 4° Impact

Although some differences are seen between the Segment 1 analysis and the Triple Segment analysis, the boundary conditions are appropriate considering the objectives of this study: structural stability of the drip shield. The drip shield will collapse when one of the sides collapse or one of the structural components fail. With the symmetry conditions causing more displacement in plate 2, collapse of the structure is more likely to occur, making the results more conservative. Although a 13 percent increase is seen in the maximum stress of plate 2, the stress is localized, indicating the results of the single segment analyses are adequate.

VI-3.2 PARAMETRIC ANALYSIS RESULTS

All 16 parametric analyses indicate that the drip shield reaches equilibrium after waste package impact without the loss of structural stability. Figures VI-18(a) to VI-33(a) illustrate the final drip shield configurations. The maximum Von-Mises stress plots presented in Figures VI-18(a) to VI-32(a) demonstrate that the stress values in bulkhead, large support beam, plate 1, and plate 2) remain within their respective material's true ultimate strength (Table 5-1). Tables VI-7 to VI-10 report the maximum Von-Mises Stress of plate 1, plate 2, the large support beam, and the bulkhead for each of the impact analyses. Table VI-11 reports the final horizontal displacement of the bottom of plate 2.

(a)

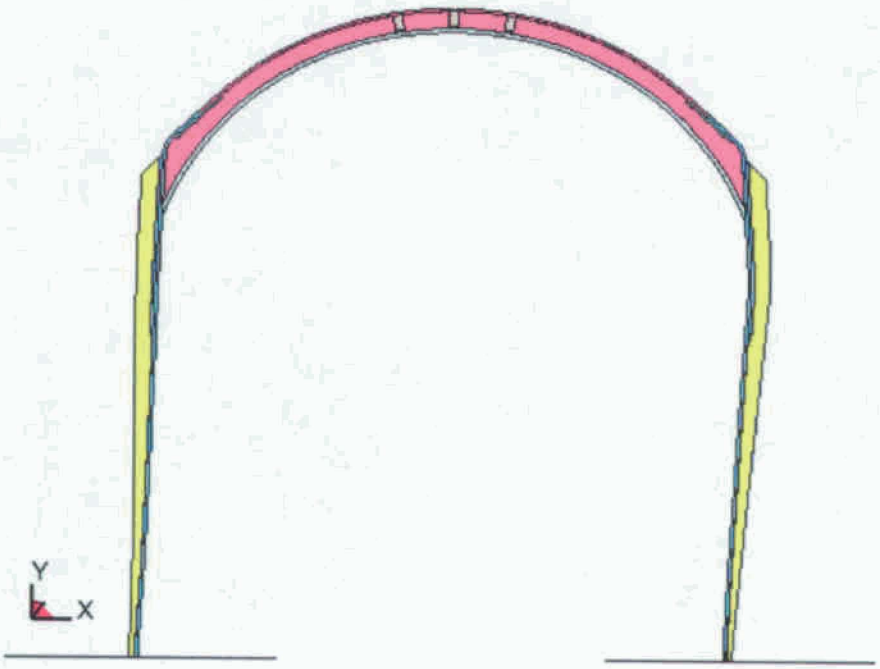

(b)

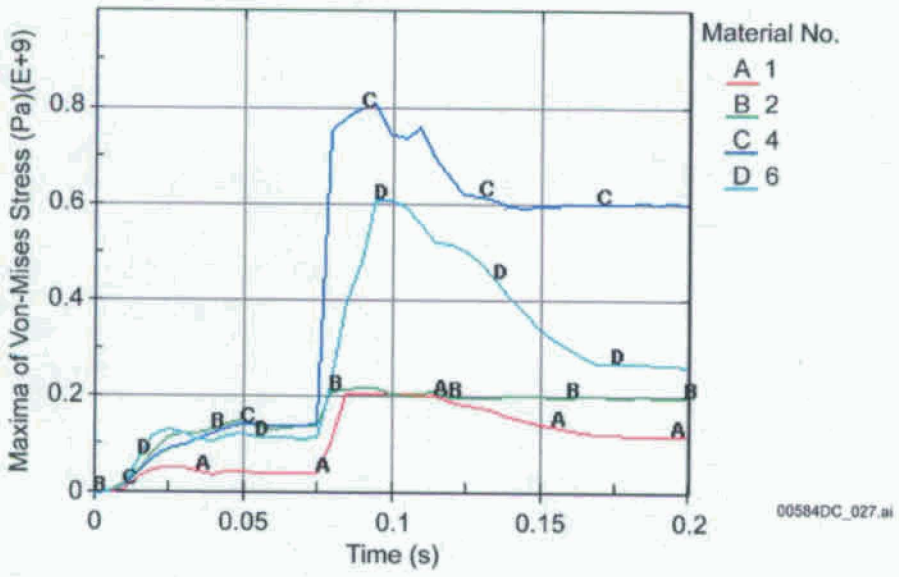

NOTE: Curve A is Plate 1, Curve B is Plate 2, Curve C is the large support beam, and Curve D is the bulkhead. See Figure VI-7.

Figure VI-18. Segment 1, 0° Direct Impact: (a) Final Drip Shield Configuration, and (b) Maximum Von-Mises Stress (Pa) in the Drip Shield Plates, Bulkhead and Large Support Beams

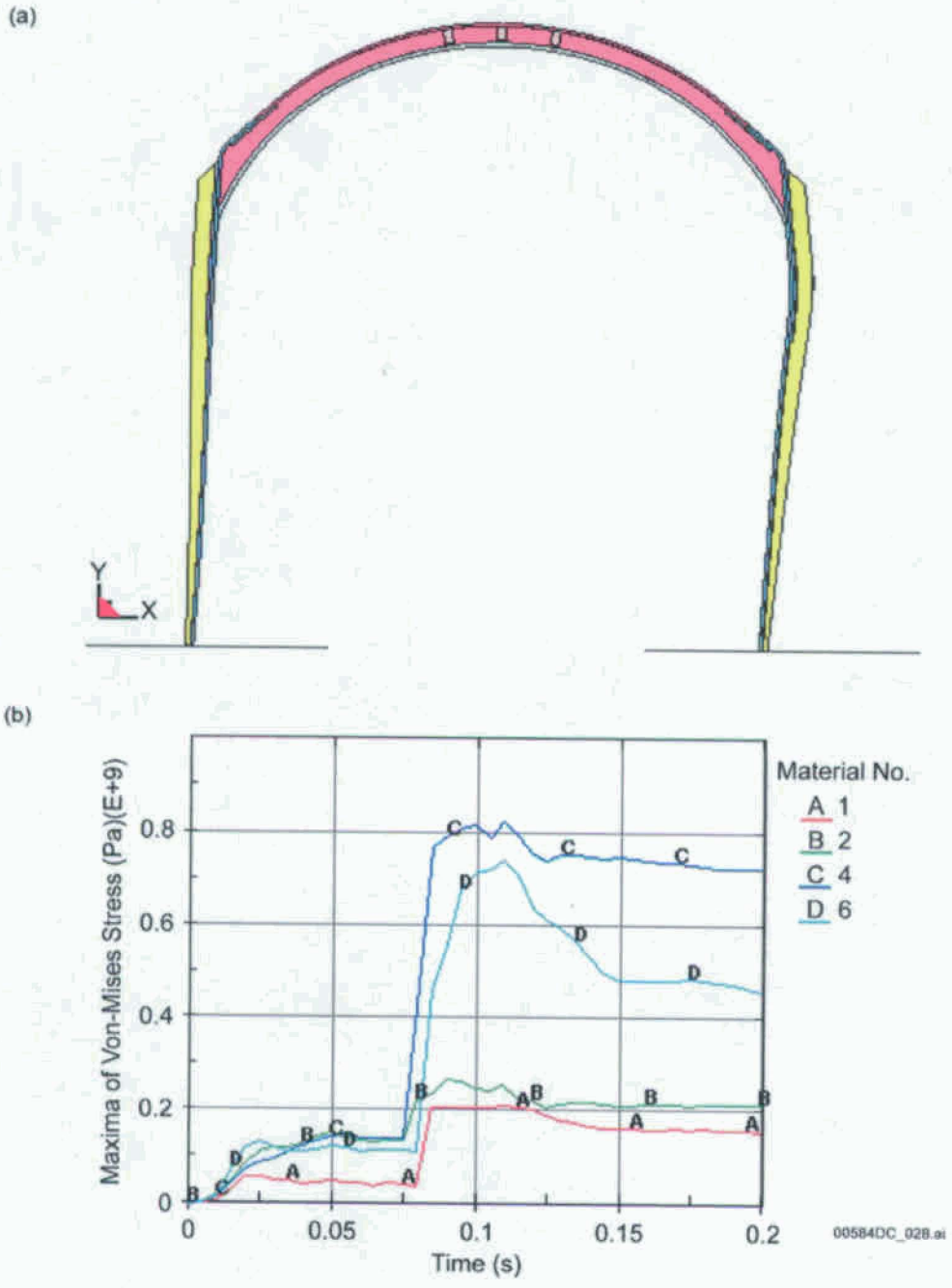

NOTE: Curve A is Plate 1, Curve B is Plate 2, Curve C is the large support beam, and Curve D is the bulkhead. See Figure VI-7.

Figure VI-19. Segment 1, 4° Direct Impact: (a) Final Drip Shield Configuration, and (b) Maximum Von-Mises Stress (Pa) in the Drip Shield Plates, Bulkhead and Large Support Beams

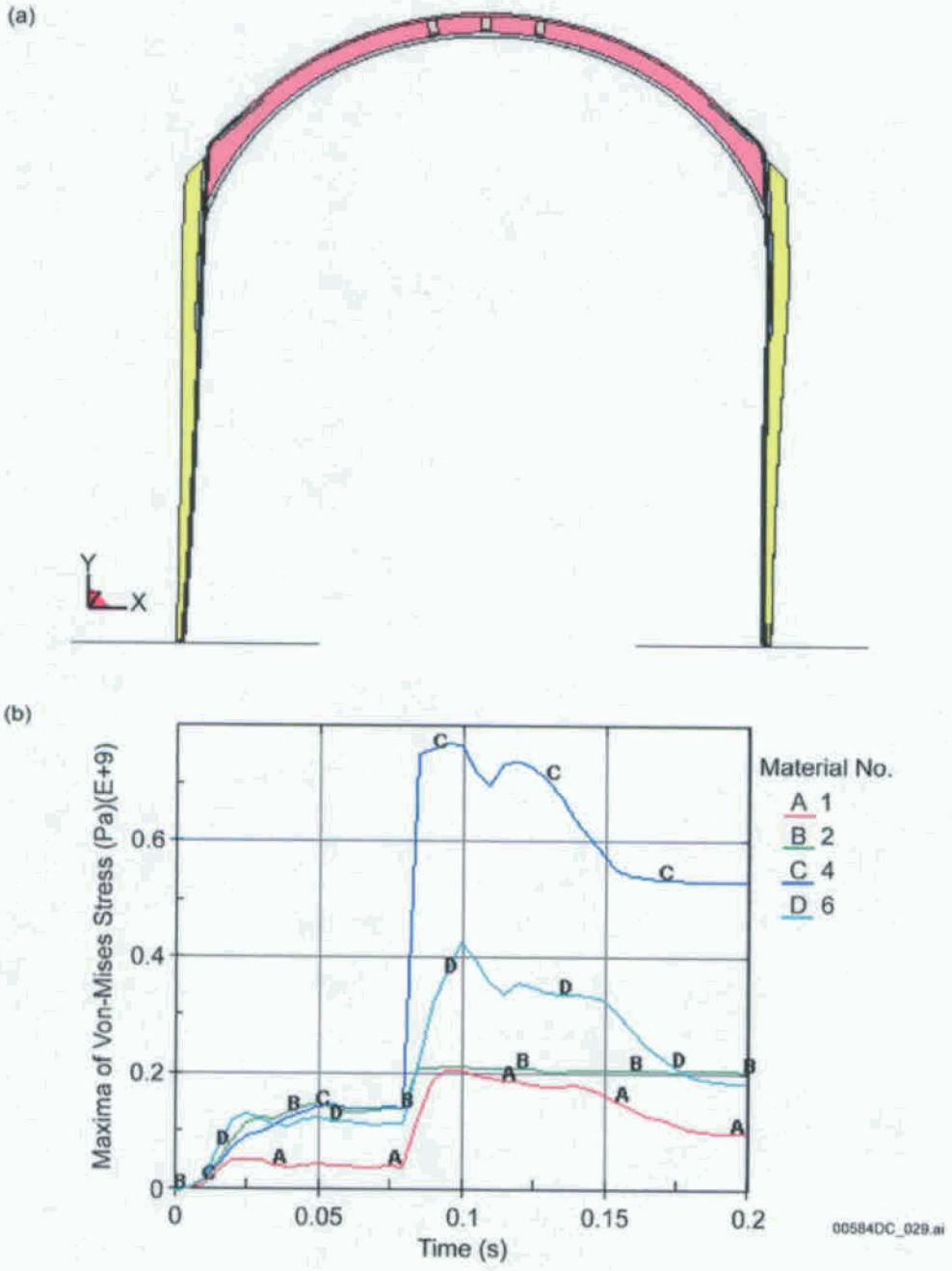

NOTE: Curve A is Plate 1, Curve B is Plate 2, Curve C is the large support beam, and Curve D is the bulkhead. See Figure VI-7.

Figure VI-20. Segment 1, 0° Oblique Impact: (a) Final Drip Shield Configuration, and (b) Maximum Von-Mises Stress (Pa) in the Drip Shield Plates, Bulkhead and Large Support Beams

(a)

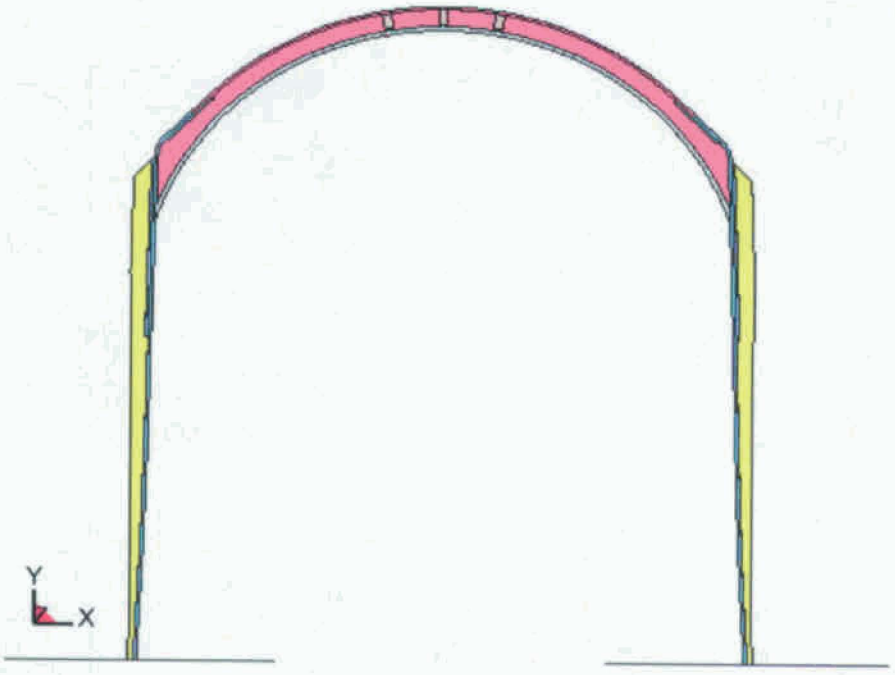

(b)

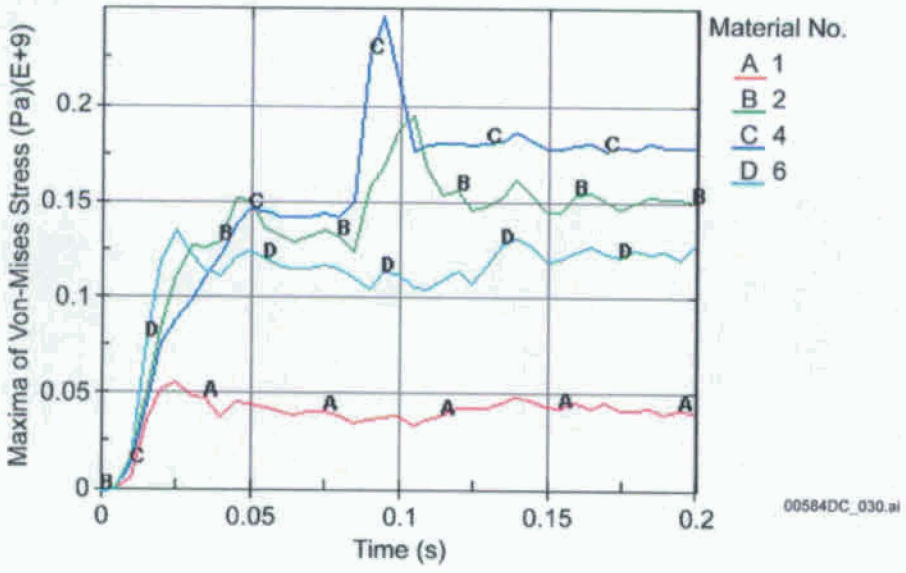

NOTE: Curve A is Plate 1, Curve B is Plate 2, Curve C is the large support beam, and Curve D is the bulkhead. See Figure VI-7.

Figure VI-21. Segment 1, 0° Glancing Impact: (a) Final Drip Shield Configuration, and (b) Maximum Von-Mises Stress (Pa) in the Drip Shield Plates, Bulkhead and Large Support Beams

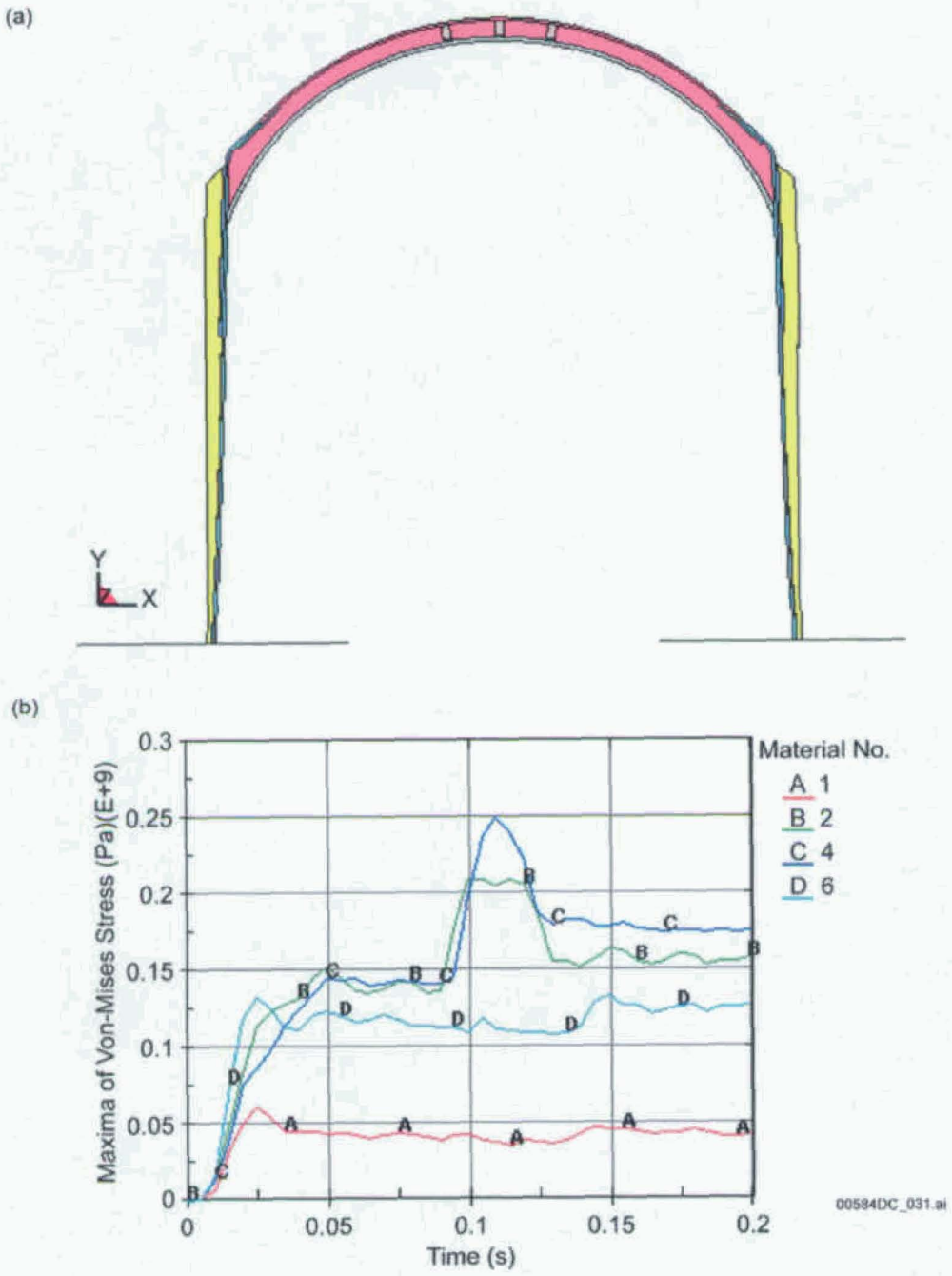

NOTE: Curve A is Plate 1, Curve B is Plate 2, Curve C is the large support beam, and Curve D is the bulkhead. See Figure VI-7.

Figure VI-22. Segment 1, 4° Glancing Impact: (a) Final Drip Shield Configuration, and (b) Maximum Von-Mises Stress (Pa) in the Drip Shield Plates, Bulkhead and Large Support Beams

(a)

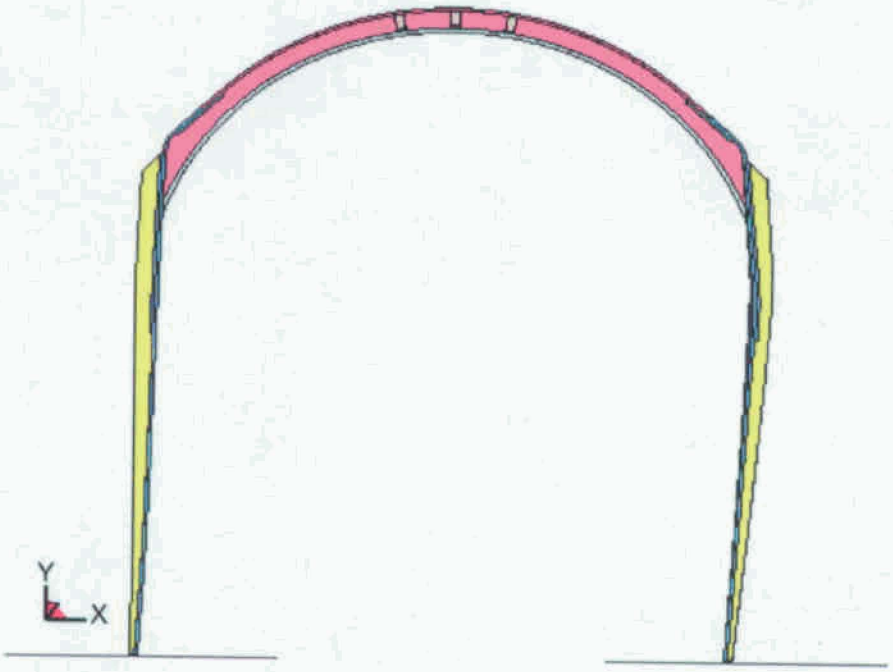

(b)

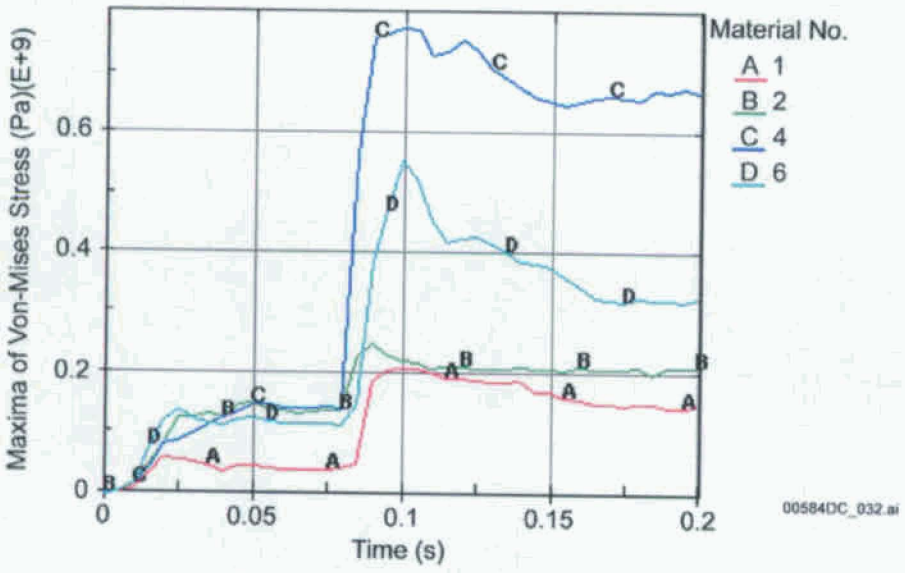

NOTE: Curve A is Plate 1, Curve B is Plate 2, Curve C is the large support beam, and Curve D is the bulkhead. See Figure VI-7.

Figure VI-23. Segment 1, 4° Oblique Impact: (a) Final Drip Shield Configuration, and (b) Maximum Von-Mises Stress (Pa) in the Drip Shield Plates, Bulkhead and Large Support Beams

(a)

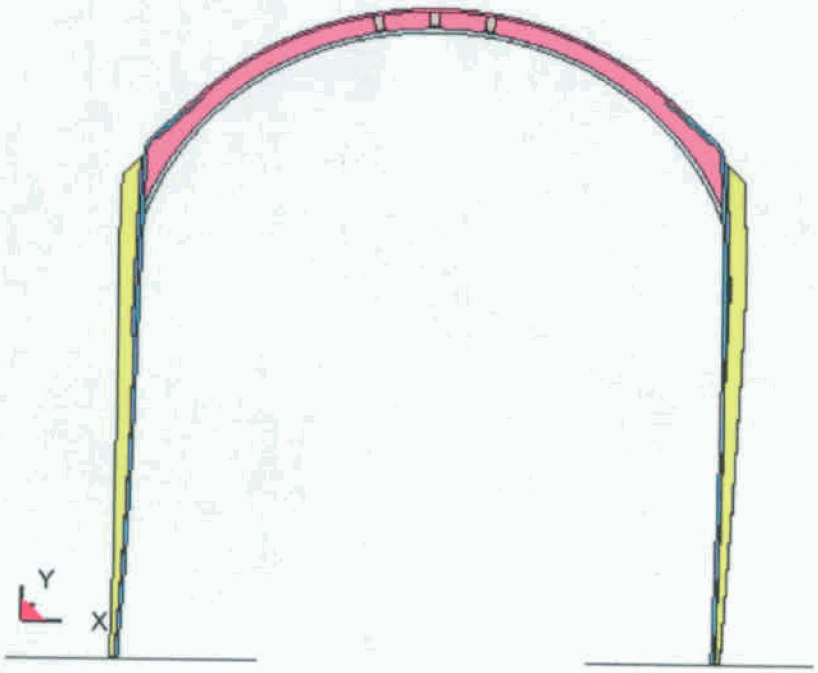

(b)

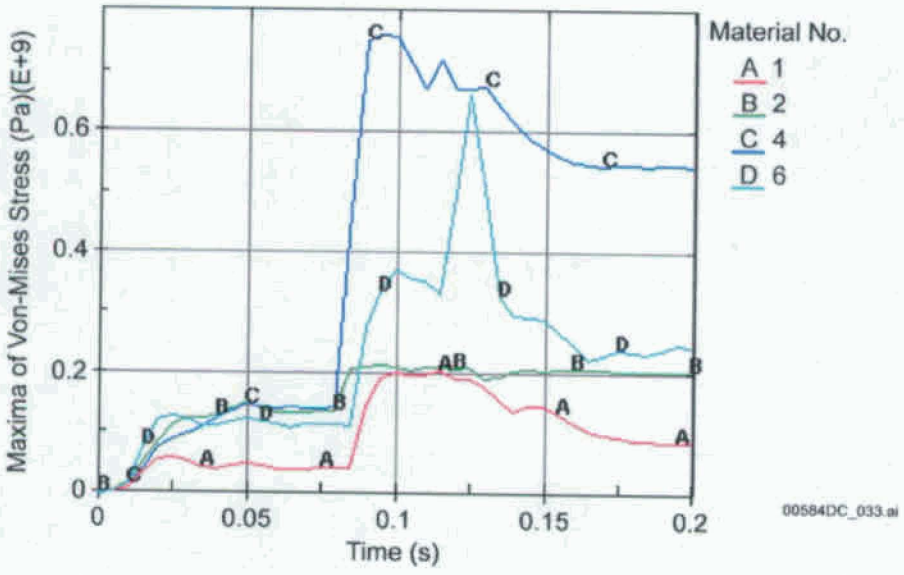

NOTE: Curve A is Plate 1, Curve B is Plate 2, Curve C is the large support beam, and Curve D is the bulkhead. See Figure VI-7.

Figure VI-24. Segment 1, 0° Rising Oblique Impact: (a) Final Drip Shield Configuration, and (b) Maximum Von-Mises Stress (Pa) in the Drip Shield Plates, Bulkhead and Large Support Beams

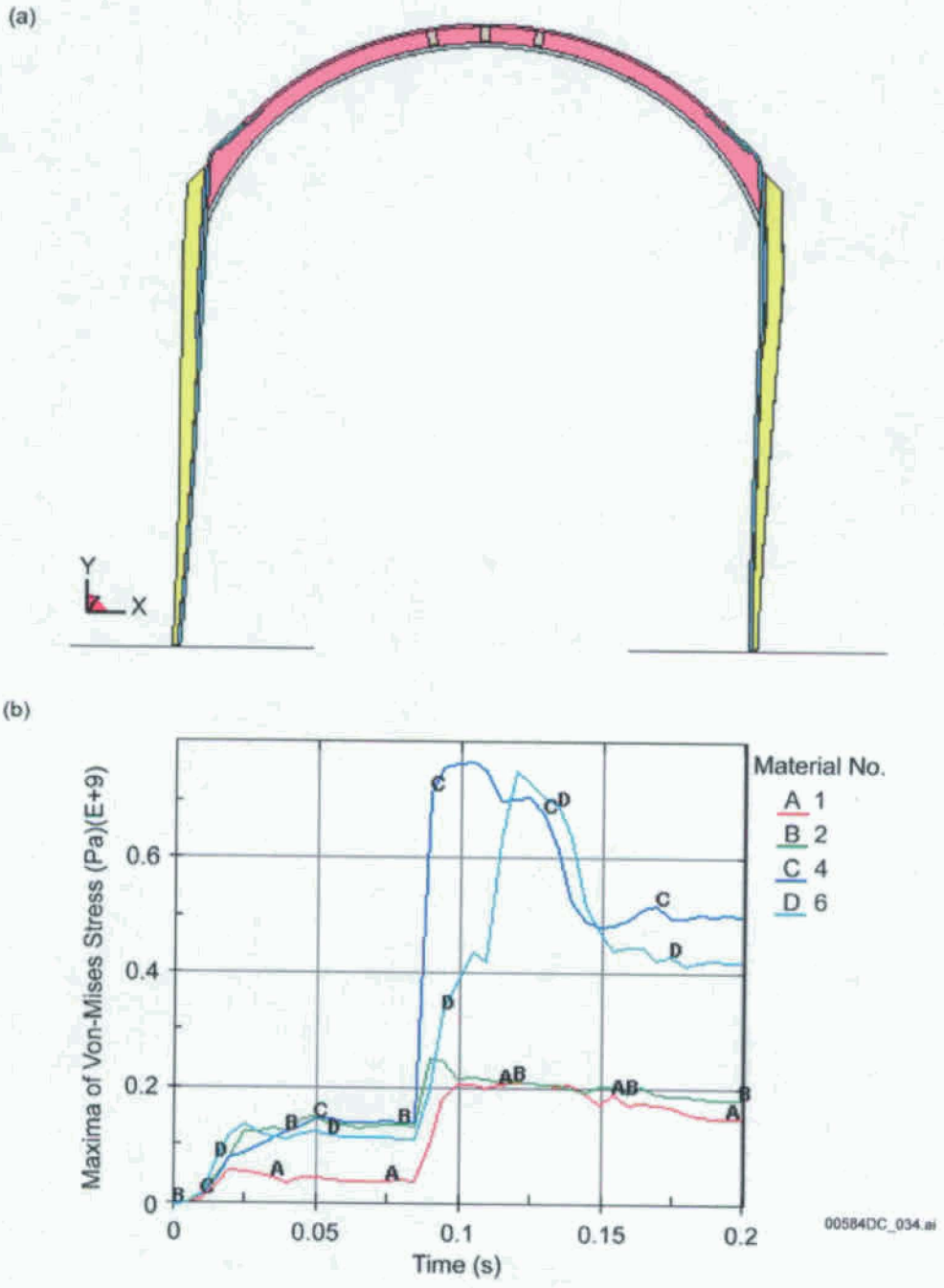

NOTE: Curve A is Plate 1, Curve B is Plate 2, Curve C is the large support beam, and Curve D is the bulkhead. See Figure VI-7.

Figure VI-25. Segment 1, 4° Rising Oblique Impact: (a) Final Drip Shield Configuration, and (b) Maximum Von-Mises Stress (Pa) in the Drip Shield Plates, Bulkhead and Large Support Beams

(a)

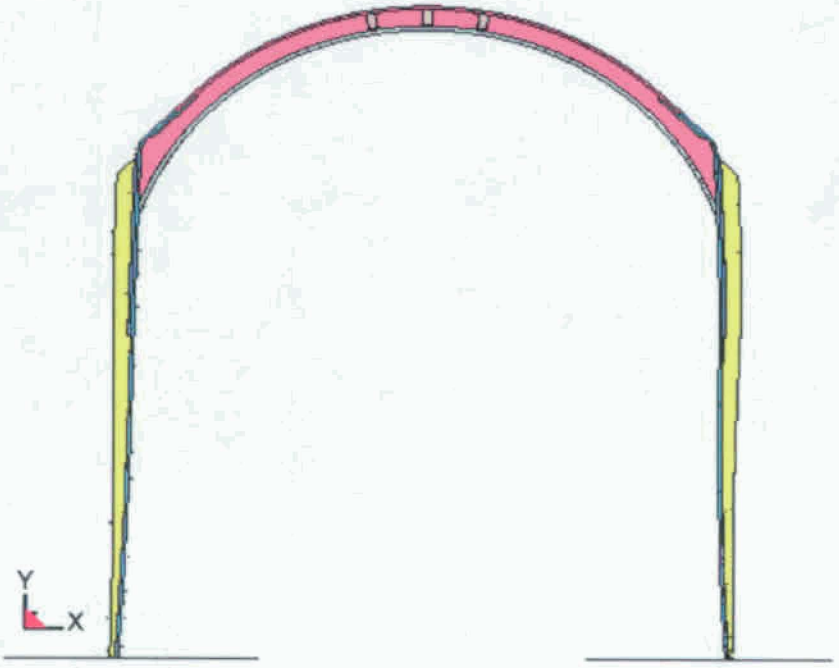

(b)

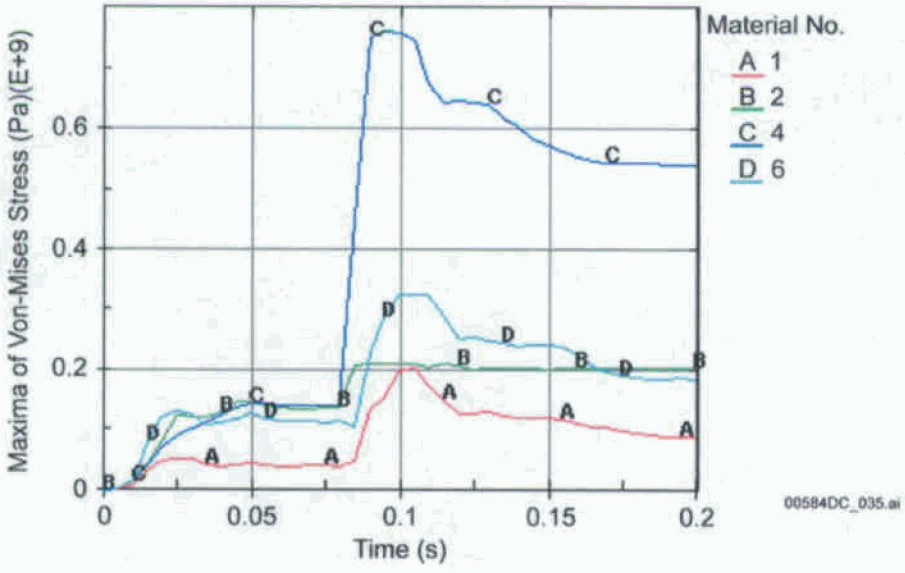

NOTE: Curve A is Plate 1, Curve B is Plate 2, Curve C is the large support beam, and Curve D is the bulkhead. See Figure VI-7.

Figure VI-26. Segment 1, 0° Falling Oblique Impact: (a) Final Drip Shield Configuration, and (b) Maximum Von-Mises Stress (Pa) in the Drip Shield Plates, Bulkhead and Large Support Beams

(a)

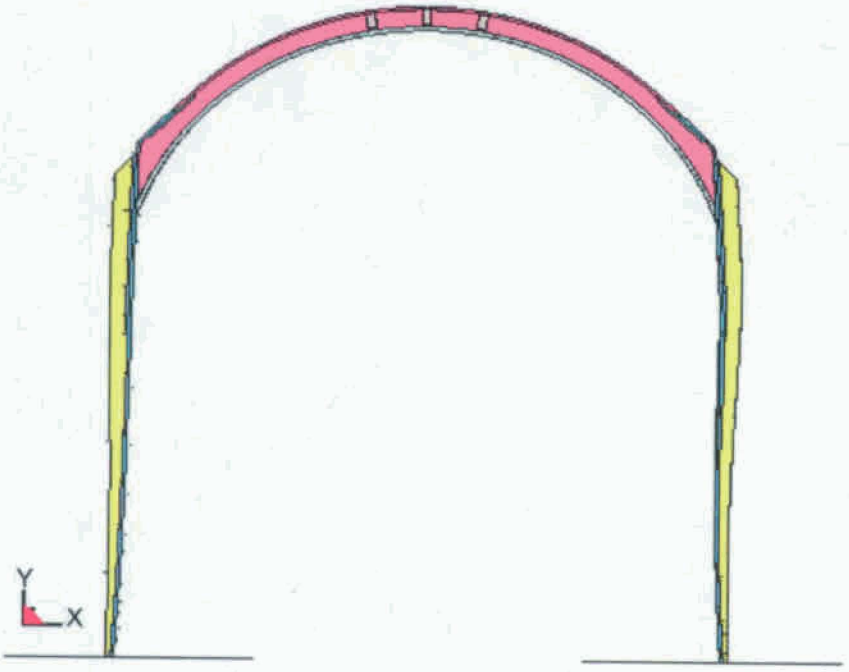

(b)

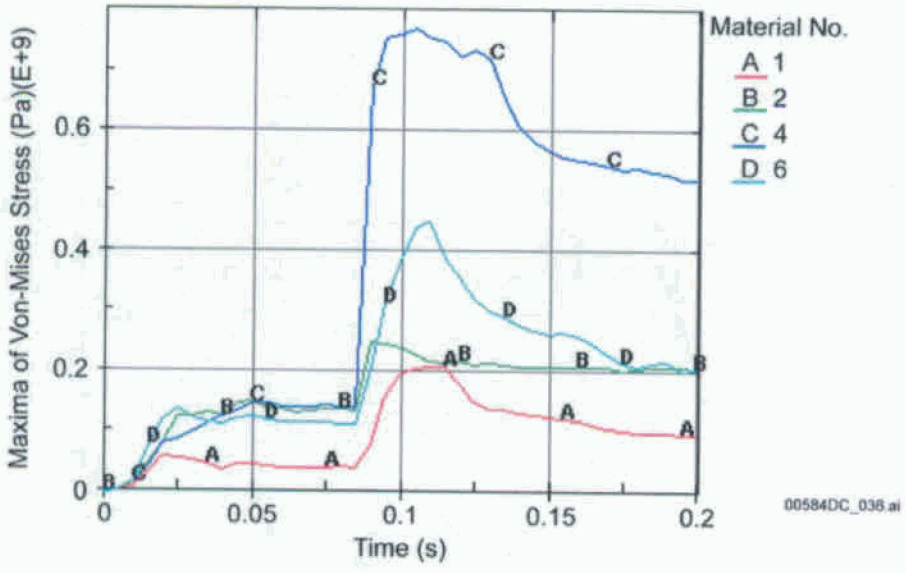

NOTE: Curve A is Plate 1, Curve B is Plate 2, Curve C is the large support beam, and Curve D is the bulkhead. See Figure VI-7.

Figure VI-27. Segment 1, 4° Falling Oblique Impact: (a) Final Drip Shield Configuration, and (b) Maximum Von-Mises Stress (Pa) in the Drip Shield Plates, Bulkhead and Large Support Beams

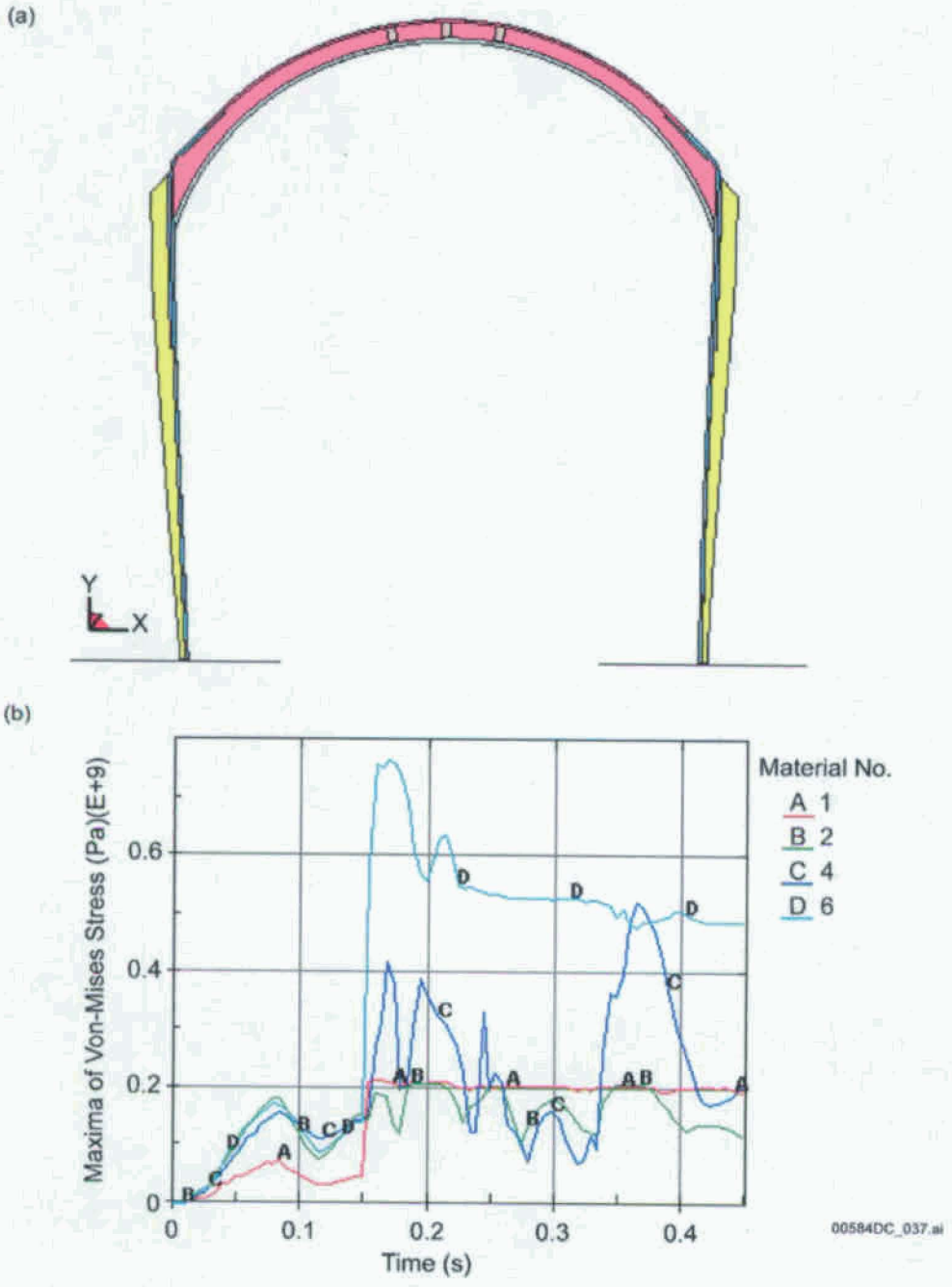

NOTE: Curve A is Plate 1, Curve B is Plate 2, Curve C is the large support beam, and Curve D is the bulkhead. See Figure VI-7.

Figure VI-28. Segment 1, Vertical Impact: (a) Final Drip Shield Configuration, and (b) Maximum Von-Mises Stress (Pa) in the Drip Shield Plates, Bulkhead and Large Support Beams

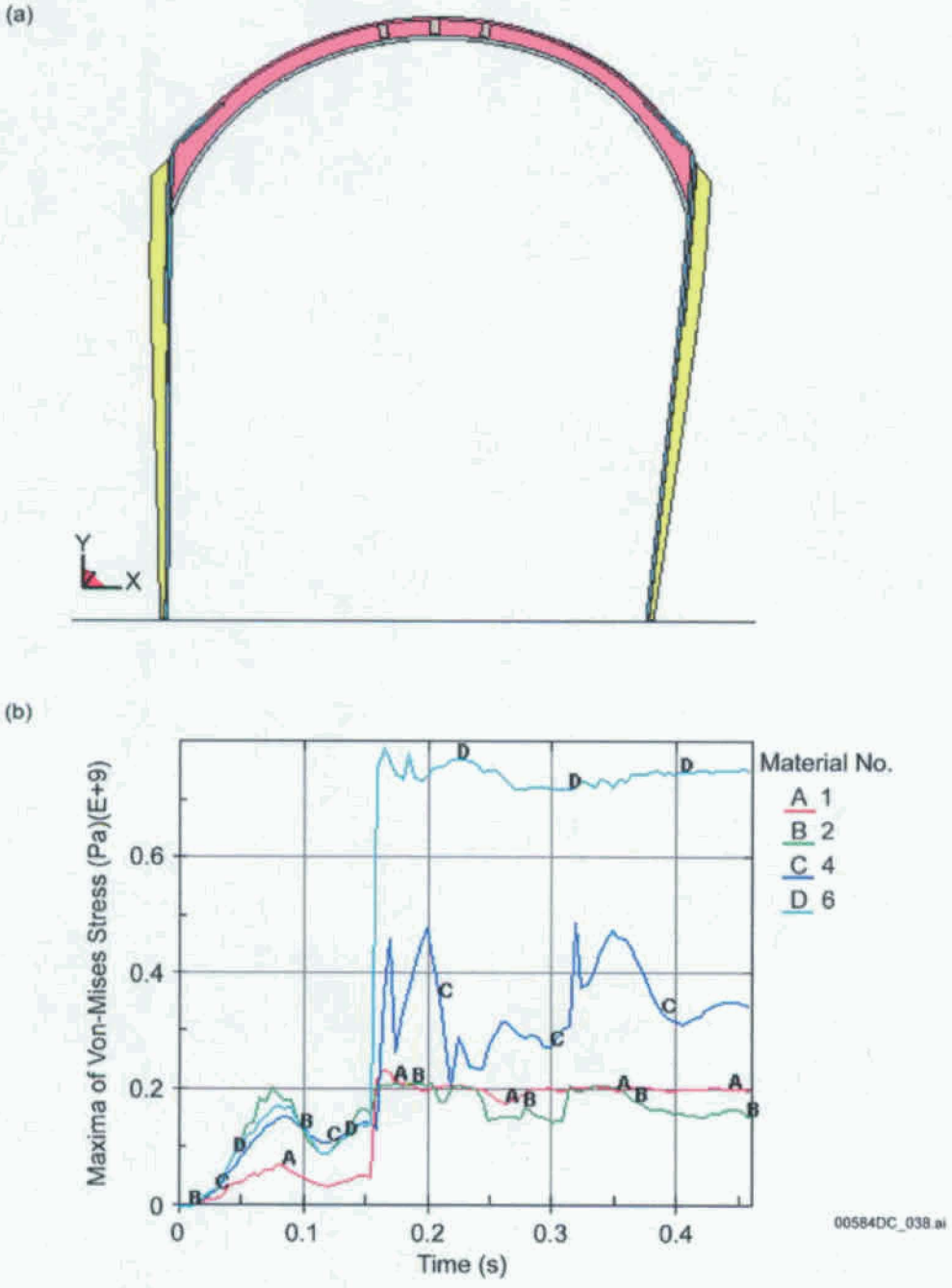

NOTE: Curve A is Plate 1, Curve B is Plate 2, Curve C is the large support beam, and Curve D is the bulkhead. See Figure VI-7.

Figure VI-29. Segment 1, Vertical-Oblique Impact: (a) Final Drip Shield Configuration, and (b) Maximum Von-Mises Stress (Pa) in the Drip Shield Plates, Bulkhead and Large Support Beams

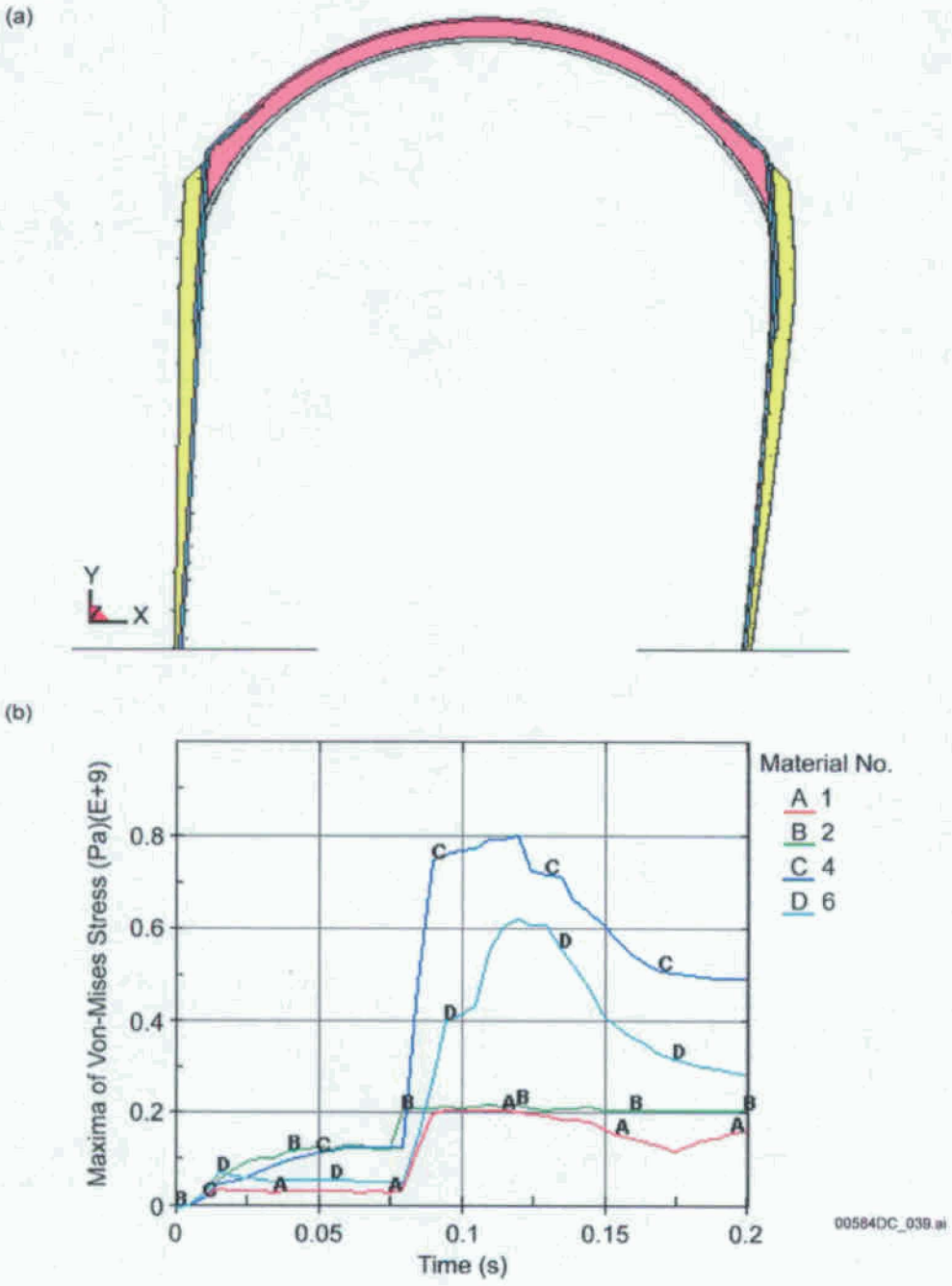

NOTE: Curve A is Plate 1, Curve B is Plate 2, Curve C is the large support beam, and Curve D is the bulkhead. See Figure VI-7.

Figure VI-30. Segment 2, 4° Direct Impact: (a) Final Drip Shield Configuration, and (b) Maximum Von-Mises Stress (Pa) in the Drip Shield Plates, Bulkhead and Large Support Beams

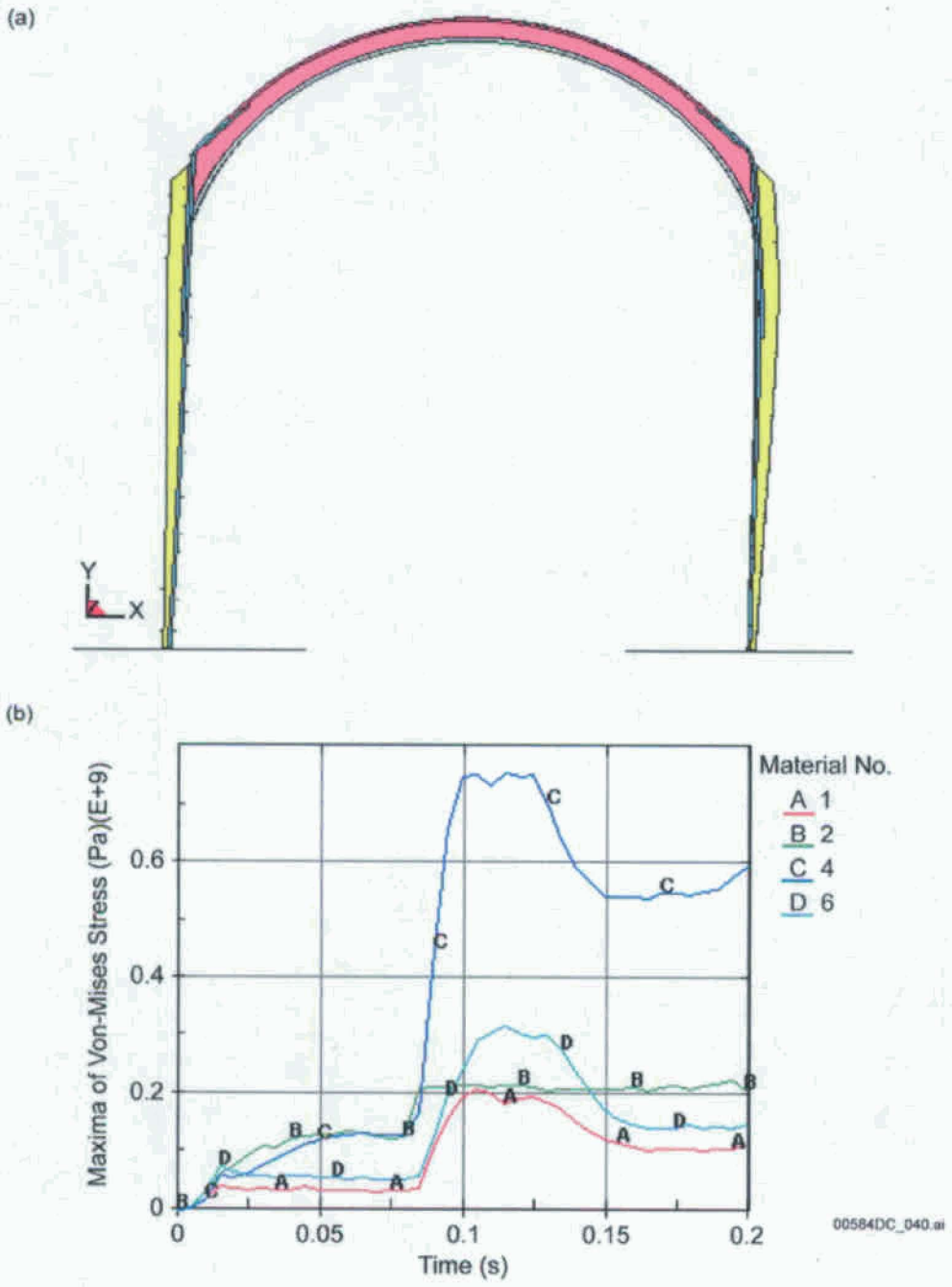

NOTE: Curve A is Plate 1, Curve B is Plate 2, Curve C is the large support beam, and Curve D is the bulkhead. See Figure VI-7.

Figure VI-31. Segment 2, 4° Oblique Impact: (a) Final Drip Shield Configuration, and (b) Maximum Von-Mises Stress (Pa) in the Drip Shield Plates, Bulkhead and Large Support Beams

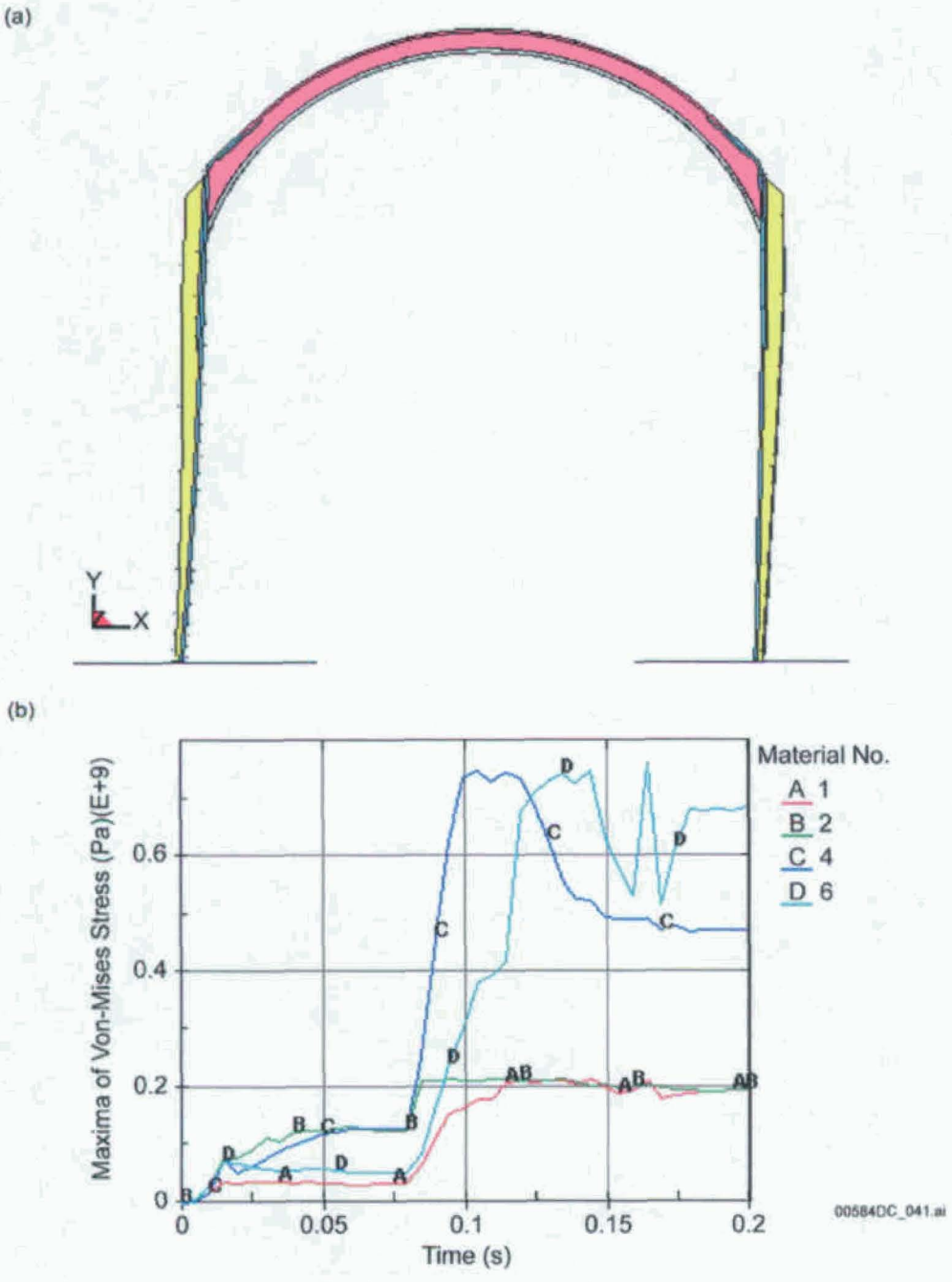

NOTE: Curve A is Plate 1, Curve B is Plate 2, Curve C is the large support beam, and Curve D is the bulkhead. See Figure VI-7.

Figure VI-32. Segment 2, 4° Rising Oblique Impact: (a) Final Drip Shield Configuration, and (b) Maximum Von-Mises Stress (Pa) in the Drip Shield Plates, Bulkhead and Large Support Beams

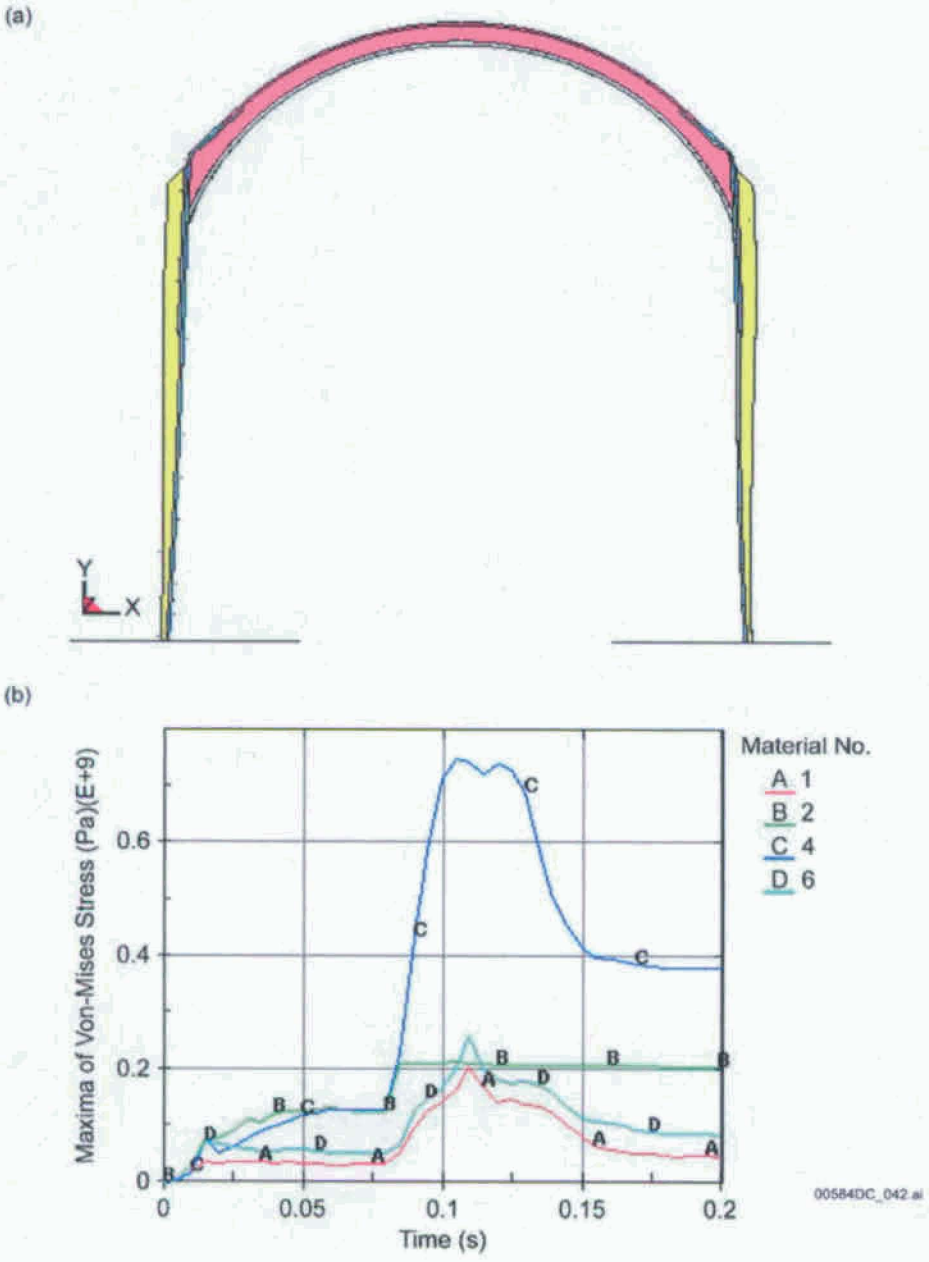

NOTE: Curve A is Plate 1, Curve B is Plate 2, Curve C is the large support beam, and Curve D is the bulkhead. See Figure VI-7.

Figure VI-33. Segment 2, 4° Falling Oblique Impact: (a) Final Drip Shield Configuration, and (b) Maximum Von-Mises Stress (Pa) in the Drip Shield Plates, Bulkhead and Large Support Beams

VI-3.3 EXTREME IMPACT VELOCITIES

Three additional simulations are performed to examine structural stability under extreme impact velocities (11 m/s). It should be emphasized that the probability of impacts of this magnitude is

role to the survivability of the drip shield: the rubble limits drip shield motion during waste package impacts, absorbs some of the impact energy, and acts as a support for the side plates during and after impacts.

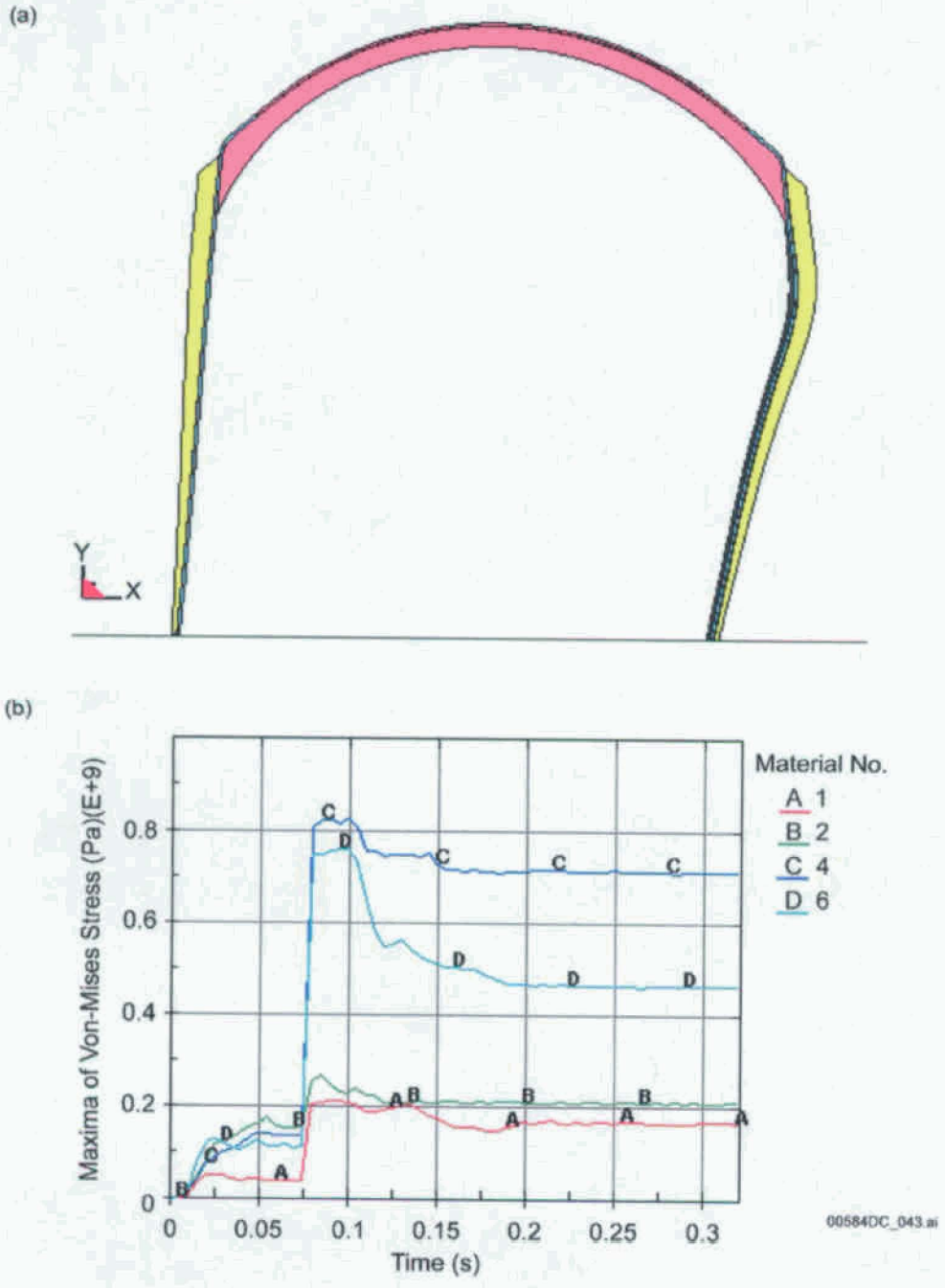

NOTE: Curve A is Plate 1, Curve B is Plate 2, Curve C is the large support beam, and Curve D is the bulkhead. See Figure VI-7.

Figure VI-35. Segment 1, 11 m/s 4° Direct Impact: (a) Final Drip Shield Configuration, and (b) Maximum Von-Mises Stress (Pa) in the Drip Shield Plates, Bulkhead and Large Support Beams

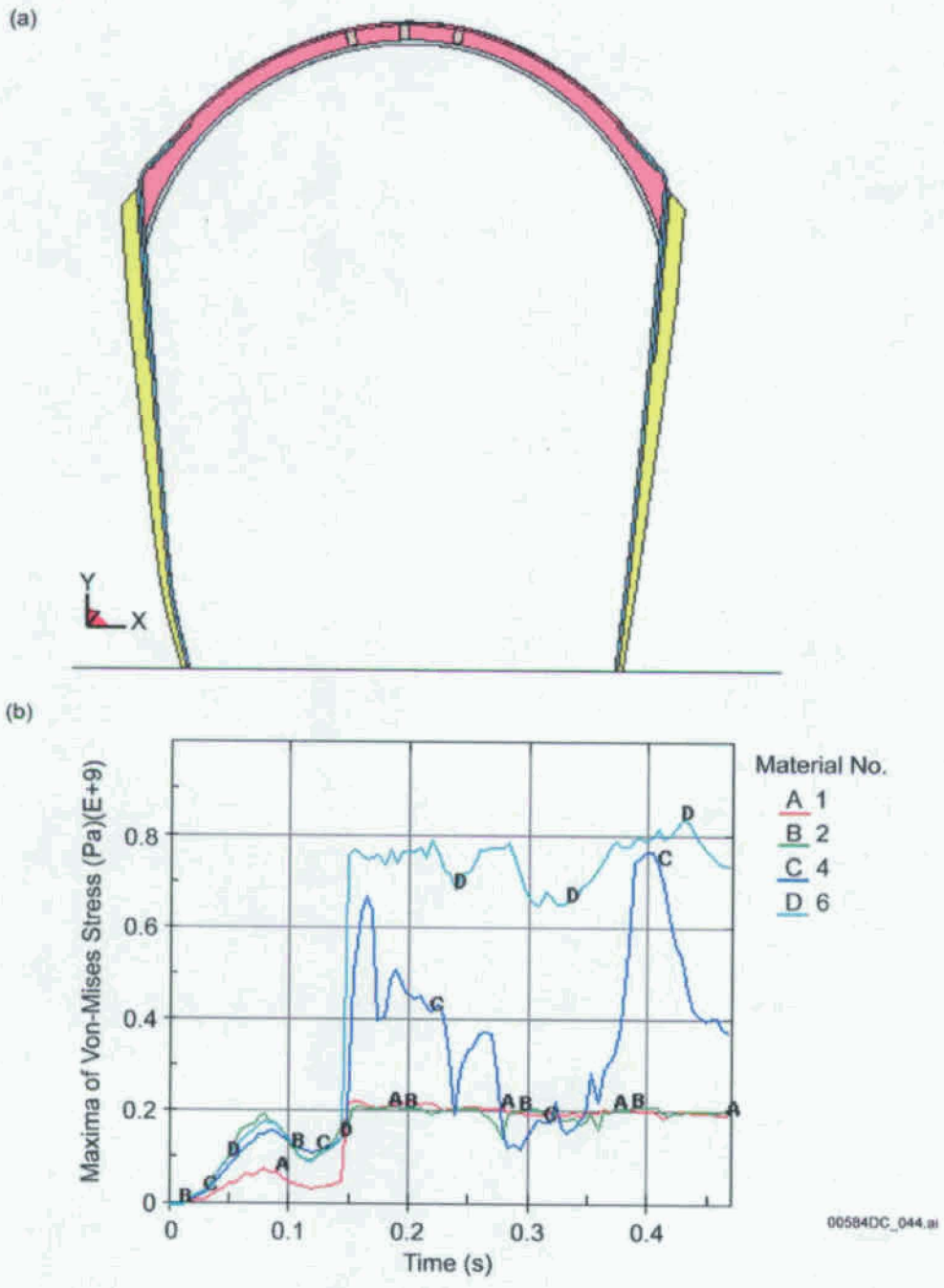

NOTE: Curve A is Plate 1, Curve B is Plate 2, Curve C is the large support beam, and Curve D is the bulkhead. See Figure VI-7.

Figure VI-36. Segment 1, 11 m/s Vertical Impact: (a) Final Drip Shield Configuration, and (b) Maximum Von-Mises Stress (Pa) in the Drip Shield Plates, Bulkhead and Large Support Beams

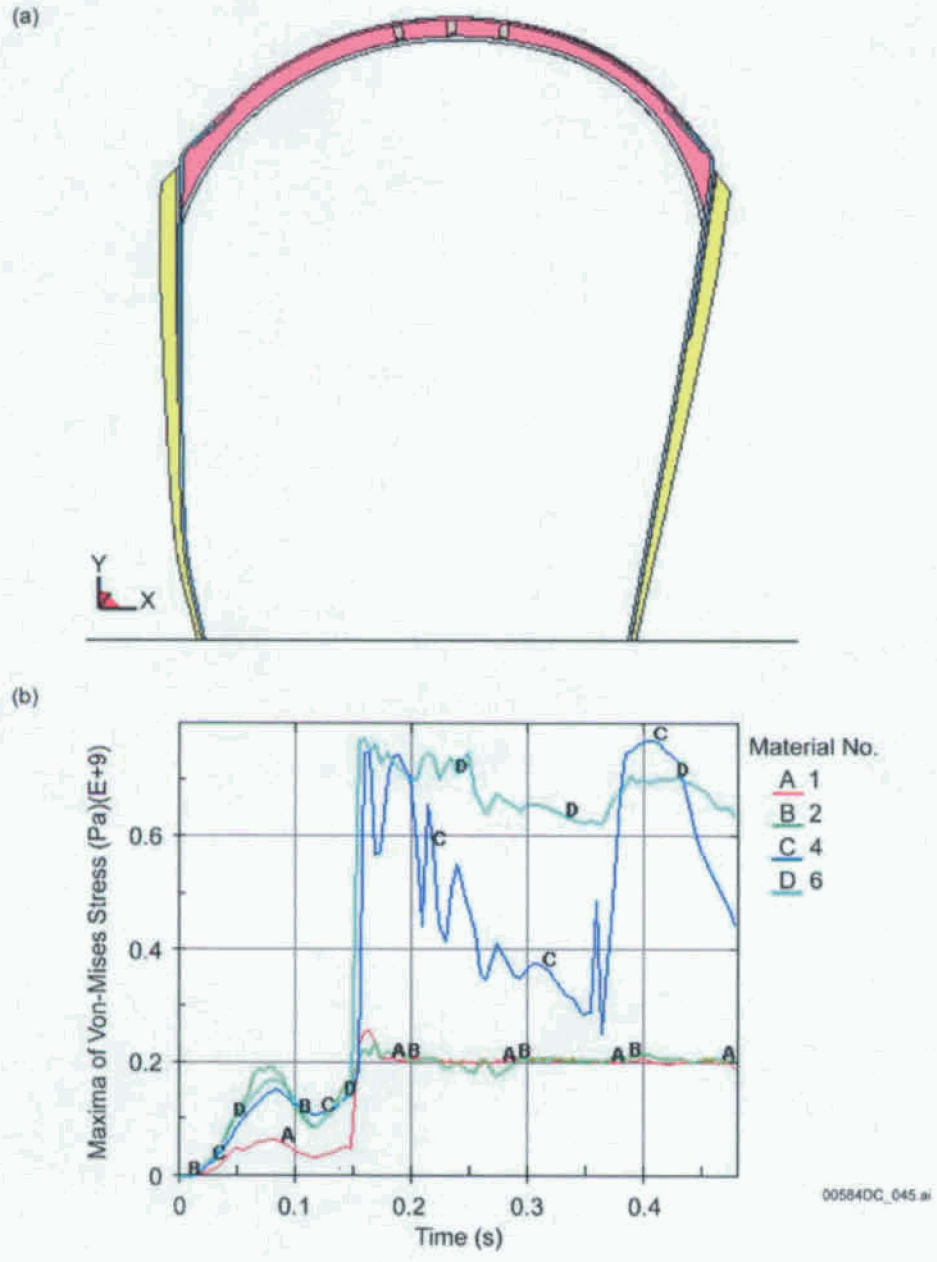

NOTE: Curve A is Plate 1, Curve B is Plate 2, Curve C is the large support beam, and Curve D is the bulkhead. See Figure VI-7.

Figure VI-37. Segment 1, 11 m/s Vertical-Oblique Impact: (a) Final Drip Shield Configuration, and (b) Maximum Von-Mises Stress (Pa) in the Drip Shield Plates, Bulkhead and Large Support Beams

VI-3.4 LONGITUDINAL IMPACTS TO THE BULKHEAD

Among the results presented in this attachment, this is the only scenario that causes a component of the drip shield to exceed its true ultimate strength. Two impact speeds were considered (1 m/s

and 2.25 m/s, see Section VI-2.1.6.4), with the impact at 2.25 m/s causing the bulkhead flange to exceed the materials true ultimate strength. Tables VI-14 and VI-15 summarize the maximum stresses and final displacements respectively. Table VI-14 shows the maximum Von-Mises stress histories for the 1 m/s and 2.25 m/s impacts; Table VI-15 shows the final horizontal displacements of the side plates. For longitudinal bulkhead impacts, the bulkhead flange plays a significant role in the analysis, and is therefore included in the Von-Mises stress plots in Figures VI-38 and VI-39. The Von-Mises stress contours are presented in Figure VI-40 for the 2.25 m/s impact. No appreciable displacements (Table VI-15) were seen in the side plate, so final configuration plots are not presented.

Table VI-14. Maximum Von-Mises Stress (MPa) for Bulkhead Longitudinal Impacts

Impact Speed	Plate 1	Plate 2	Large Support Beam	Bulkhead	Bulkhead Flange
1 m/s	214	214	372	787	932
2.25 m/s	232	231	732	979	1,323

Table VI-15. Final Horizontal Displacement (m) of the Drip Shield Side Plates for Bulkhead Longitudinal Impacts

	Absolute		Relative to Rubble	
Impact Speed	Left	Right	Left	Right
1 m/s	0.000	0.000	0.000	0.000
2.25 m/s	0.000	0.006	0.000	0.002

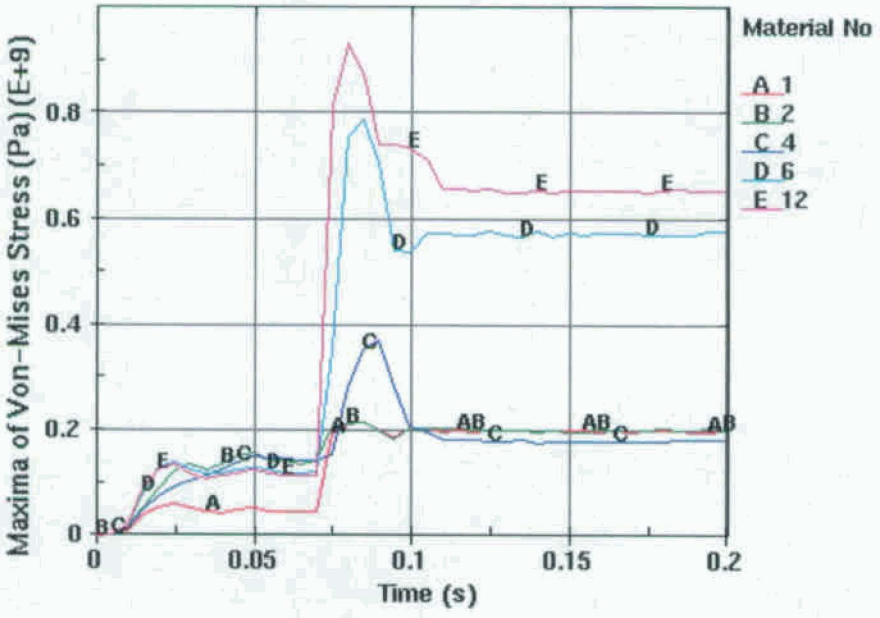

NOTE: Curve A is Plate 1, Curve B is Plate 2, Curve C is the large support beam, and Curve D is the bulkhead, and Curve E is the bulkhead flange. See Figures VI-6 and VI-7.

Figure VI-38. Longitudinal Bulkhead Impact (1 m/s) Maximum Von-Mises Stress (Pa)

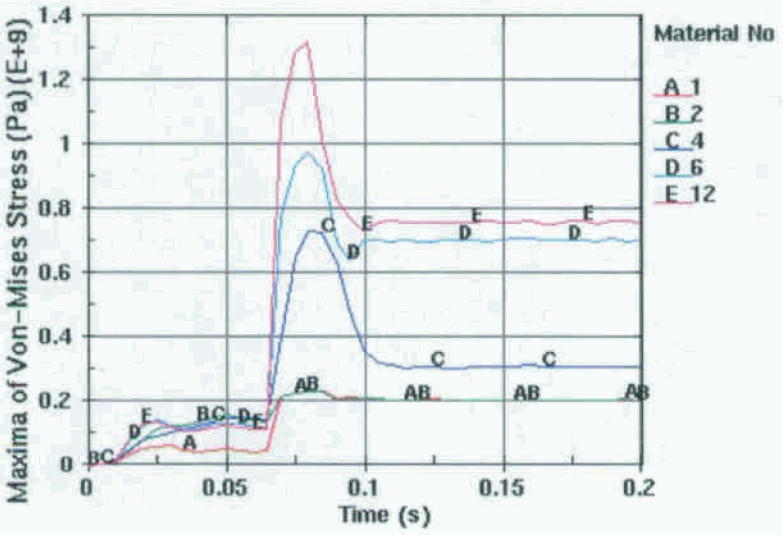

NOTE: Curve A is Plate 1, Curve B is Plate 2, Curve C is the large support beam, and Curve D is the bulkhead, and Curve E is the bulkhead flange. See Figures VI-6 and VI-7.

Figure VI-39. Longitudinal Bulkhead Impact (2.25 m/s) Maximum Von-Mises Stress (Pa)

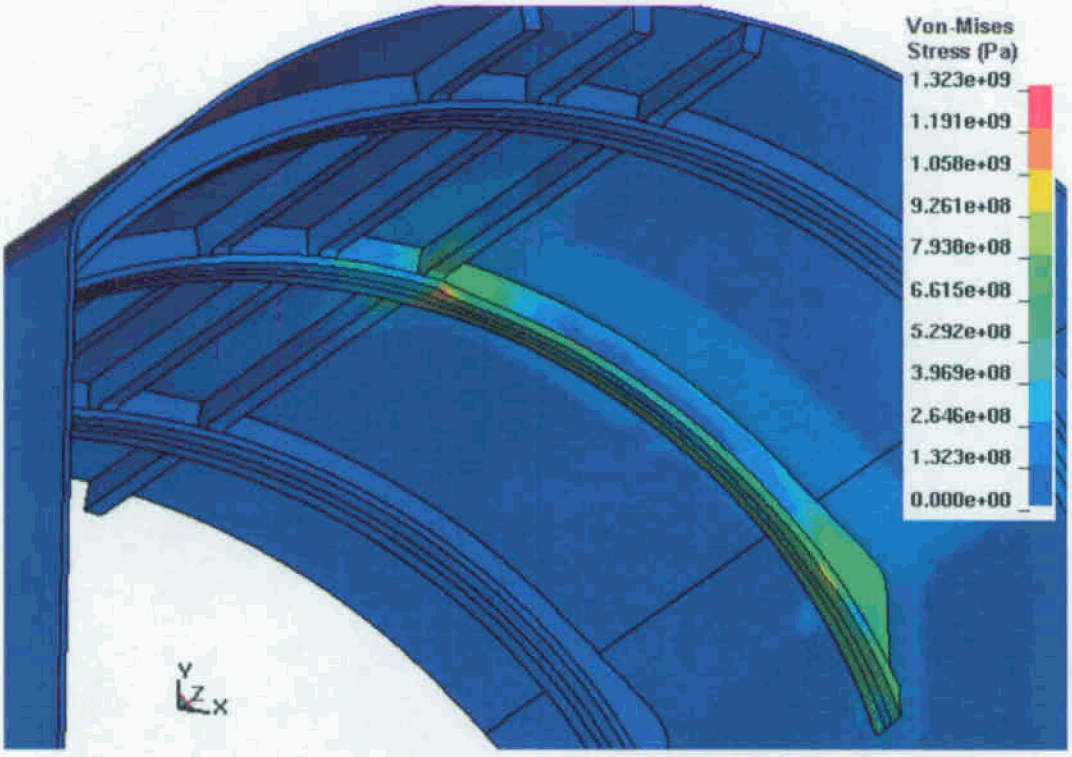

Figure VI-40. Von-Mises Stress Contours (Pa) Resulting from a 2.25 m/s Longitudinal Impact to the Bulkhead (Internal Support Plate Not Shown; time = 0.08 seconds)

The maximum stress occurs at the juncture where a longitudinal stiffener meets the bulkhead (Figure VI-40). This is also the location where the waste package makes contact with the flange.

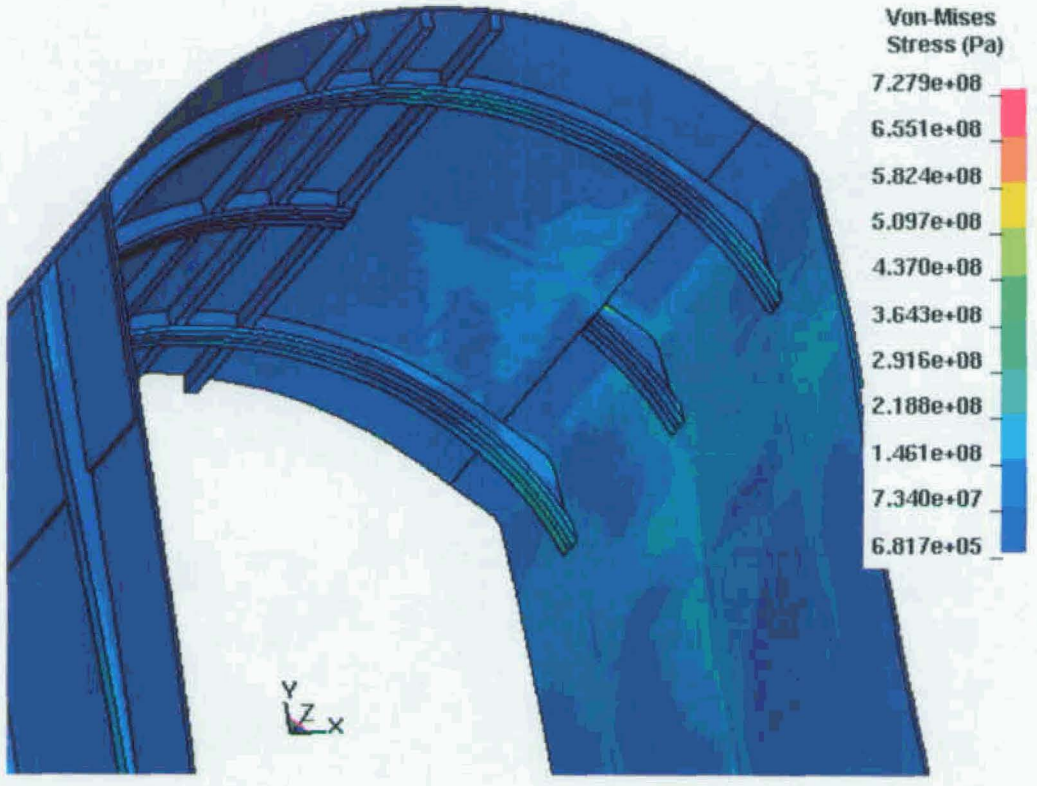

Figure VI-41. Von-Mises Stress Contours (Pa) Resulting From a 6 m/s Direct 4° Impact to the Triple Segment Analysis Missing a Section of the Center Bulkhead (Internal Support Plate Not Shown; time = 0.25 seconds)

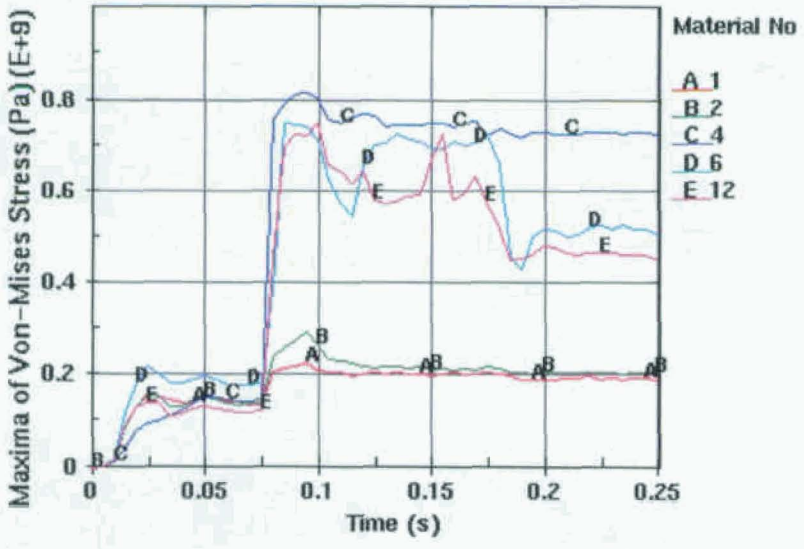

NOTE: Curve A is Plate 1, Curve B is Plate 2, Curve C is the large support beam, and Curve D is the bulkhead, and Curve E is the bulkhead flange. See Figures VI-6 and VI-7.

Figure VI-42. Direct 4° Impact (6 m/s) to the Triple Segment Analysis Missing a Section of the Center Bulkhead Maximum Von-Mises Stress (Pa)

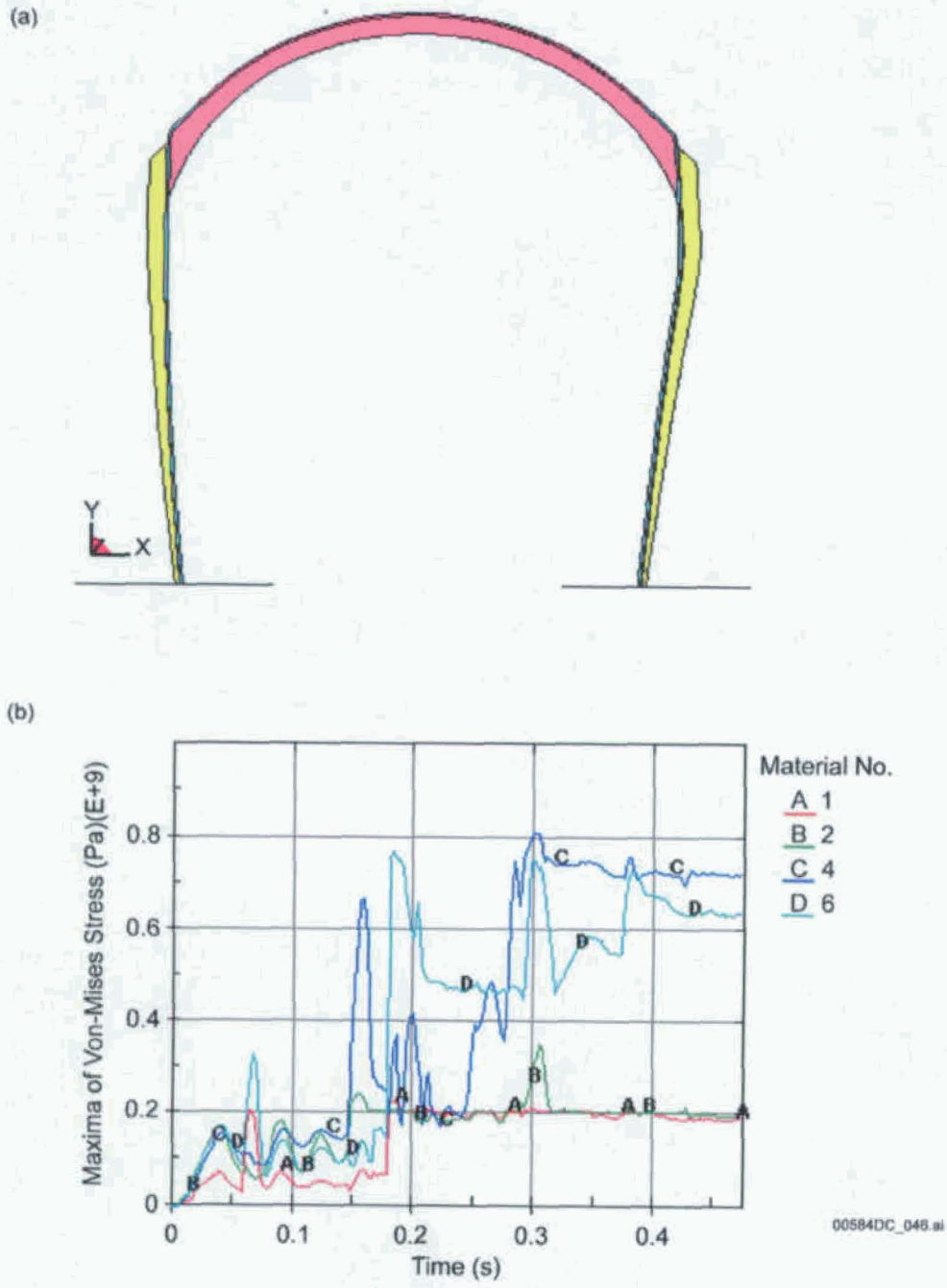

NOTE: Curve A is Plate 1, Curve B is Plate 2, Curve C is the large support beam, and Curve D is the bulkhead. See Figure VI-7.

Figure VI-44. Multiple Impact Scenario: (a) Final Drip Shield Configuration, and (b) Maximum Von-Mises Stress (Pa) in the Drip Shield Plates, Bulkhead and Large Support Beams

at the final stages of the tests are shown in Figures IX-3 and IX-4 for constant confinement and uniaxial strain loading conditions, respectively. The biaxial stress tests were conducted for different magnitudes of confinement, including 0.05 MPa, 0.1 MPa, 0.5 MPa and 1.0 MPa. (Unconfined compression experiments were not conducted because granular materials theoretically have zero strength under unconfined conditions.) The geometry of the samples taken from sample extraction windows 1, 2 and 3, indicated in Figure IX-1, and sets of stress-strain curves (in each set, 4 curves are presented for different biaxial confining stresses and 1 curve is for uniaxial strain loading conditions) for each sample are shown in Figures IX-5 through IX-10. The average porosities of the samples from sample extraction windows 1, 2 and 3 are 11.2 percent, 11.9 percent and 6.9 percent, respectively. The directional dependence of the deformability was investigated by loading the sample from extraction window 1 in the vertical and horizontal directions. In fact, in the second case, the loading was still in the vertical direction, but the sample was rotated by 90 degrees. The sample geometry for this case and the stress-strain curves obtained are shown in Figures IX-11 and IX-12. Finally, the effect of the initial rock mass-quality was investigated by testing the sample from extraction window 1 using the mechanical properties of the UDEC analysis that correspond to a category 4 lithophysal rock mass. The calculated stress-strain curves are shown in Figure IX-13.

The numerical results qualitatively show expected trends. The strength and stiffness of the samples increase as confinement increases. For very low confinement the strength and the stiffness converge to zero. This demonstrates that the sample size is sufficient; otherwise, were there a size effect, the samples would have finite strength for unconfined conditions. The curves for a uniaxial strain condition have a typical, hyperbolic, continuously hardening, concave upward shape.

An unexpected result is that the sample taken from extraction window 3, with the smallest porosity of 6.9 percent, exhibits the softest response. One possible explanation for this is that extraction window 3 lies on the vertical axis of symmetry of the drift, resulting in a particular distribution of voids between the blocks; when these blocks are loaded vertically, a relatively soft response results. One test of directional dependence of stiffness indicates that there is an anisotropy of the deformability of the rubble. Although the locations and size of the samples were selected such that porosity inside the sample is relatively uniform, it does vary. This variability might be affecting the results, but a more probable explanation of the anisotropy is the predominantly unidirectional (vertical) movement of the blocks during the collapse.